

Conductivity and dielectric behavior of PEO-PAM-NaCF₃SO₃ blend electrolyte system irradiated with swift heavy O⁶⁺ ion beam

Gargi Dave^a, Dinesh Kanchan^{a,*}, Fouran Singh^b

^a Solid State Ionics and Glass research Laboratory, Department of Physics, Faculty of Science, The Maharaja Sayajirao University of Baroda, Gujarat, India

^b Inter-University Accelerator Centre (IUAC), Aruna Asaf Ali Marg, New Delhi, India

ARTICLE INFO

Keywords:

Blend electrolyte system
SHI irradiation
Ionic conductivity
Dielectric properties

ABSTRACT

Blend Polymer Electrolyte (BPE) system of Polyethylene Oxide and Polyacrylamide (PEO-PAM) with Sodium trifluoromethanesulfonate (NaCF₃SO₃) salt has been exposed to Swift Heavy Ion (SHI) beam irradiation. Irradiation with swift heavy oxygen beam has been performed at four different fluences of 1×10^{11} ions/cm², 3×10^{11} ions/cm², 1×10^{12} ions/cm² and 2×10^{12} ions/cm². BPE films are made by solution cast method. Electrochemical properties of non-irradiated and irradiated samples have been studied using impedance spectroscopic technique in the frequency range 20 Hz–2 MHz from ambient temperature to 333 K. Fourier transform infrared spectroscopy (FT-IR) and scanning electron microscopy (SEM) have been performed to characterize the films to understand the molecular structure and surface morphology of the electrolyte films. From impedance analysis, it is observed that ionic conductivity increases with increase in fluence and maximum room temperature conductivity is found to be 5×10^{-5} S/cm at a fluence of 1×10^{12} ions/cm² and but decreases by irradiating at 2×10^{12} ions/cm² fluence. Dielectric relaxation, $\tan\delta$ and modulus formalism of the system before and after irradiation has been discussed in the paper.

1. Introduction

Solid Polymer Electrolyte (SPEs) for applications in solid state batteries are very important because of their outstanding advantages like leak-proof nature, light weight, ease of fabrication into desired geometries, high energy density and good mechanical strength (Nath and Kumar, 2010; Subramaniam and Lu, 2011; Ngai et al., 2016; Marinov et al., 2017). Sodium-ion electrolytes are investigated widely due to its material abundance, low cost and environment friendly nature (Marinov et al., 2017; Vélez et al., 2017; Vignarooban et al., 2016; Wang et al., 2015a, 2015b). PEO (Polyethylene Oxide), has been extensively investigated as host matrix for SPEs ever since Armand (Armand et al., 1979) showed its commercial applicability as electrolyte material. Reports are available on PEO-Na⁺ salt complexes, i.e., Morena et al. (2014) have studied electrochemical characterization of PEO-NaTFSI polymer electrolyte and Chandra et al. (2011) have studied ion conduction mechanism on PEO-NaHCO₃ electrolytes. PEO-NaClO₄ polymer complexes have been studied by Nimah et al. (2015) whereas, Sapri and Ahmad (2015) have studied PEO-NaCF₃SO₃ solid polymer electrolyte films (Sharma et al., 2013b; Wang et al., 2015a, 2015b; Gohel and Kanchan, 2018). Presence of plasticizer in the polymer host, in pure PEO/salt complexes, PEO exists in crystalline, amorphous and

in a mixed phase (Marinov et al., 2017). In polyethylene oxide, the valence electrons are bound in sp³ hybridized covalent bonds. The mobility in PEO is very low, hence do not contribute to the electrical conductivity of the material and PEO based electrolytes generally suffer from poor ambient temperature conductivity (10^{-7} to 10^{-8} S/cm) due to the presence of such crystalline regions (Kumar et al., 2011). Several approaches are being investigated to achieve higher ionic conduction in PEO-salt complexes like blending of two or more polymers (Liang et al., 2015; Sharma et al., 2013a), addition of high dielectric constant plasticizers like EC, PC, DEC, PEG (Sharma et al., 2013; Wang et al., 2015a, 2015b; Gohel et al., 2018). In presence of plasticizer, polymer electrolyte exhibits high ambient temperature ionic conductivity. However, such plasticized films show poor mechanical properties at high plasticizer content. If inert nano-fillers such as Al₂O₃, TiO₂, SiO₂ (Nimah et al., 2015; Pitawala et al., 2007; Hema and Tamilselvi, 2016) are molecularly dispersed within a polymer matrix, these fillers not only reduce the crystallinity of host polymers, resulting in higher ionic conductivity but also maintain the mechanical strength of the polymer matrix. By incorporation of ionic liquids (Monti et al., 2016; Hasa et al., 2016), irradiating with γ -rays (Nanda et al., 2010; Raghu et al., 2016), ion beams (Delgado et al., 2009; Kim et al., 2011;), electron beam (Raghu et al., 2016, 2014), x-rays (Papoutsaki et al., 2013) and swift

* Corresponding author.

E-mail address: dk.kanchan-phy@gmail.com (D. Kanchan).

<https://doi.org/10.1016/j.radphyschem.2019.03.019>

Received 18 September 2018; Received in revised form 26 February 2019; Accepted 14 March 2019

Available online 19 March 2019

0969-806X/ © 2019 Elsevier Ltd. All rights reserved.

heavy ion (SHI) beam (Abdul-Kader et al., 2012; Joge et al., 2014; Dave et al., 2018; Kumar et al., 2006) also help in modification of polymer matrix and facilitate in enhancing the ionic conductivity.

During irradiation through the material, beam imparts its energy to the matter which can be interpreted in terms of two types of stopping power (dE/dx). One, nuclear stopping power due to low energy ion beam, which displaces the atoms of the material and two, electron stopping power due to high energy ion beam, which travels a straight line path creating damaged zones on its way. Because of their large range, swift heavy ions are not embedded into the material. Ion irradiation by SHI prompts changes in irreversible structural modifications in polymers which depend on ion fluence and electronic energy loss S_e . It is observed that, at low fluence, small value of electronic energy brings a decrease in free volume or enhances the densification. Beyond a certain S_e value, SHI produces low density along its trajectory and different events like bond cleavage, ionization, chains scissioning, cross-linking and mass losses give rise to structural modifications in polymers. Lakshmi et al (Lakshmi et al., 2008) studied the effect of C^{5+} ion beam irradiation on optical and electrical properties of PmT-PVC and *p*-TSA-PoT-PVC blend system whereas Joge et al have (Joge et al., 2014) have described conductivity and relaxation mechanism in PEO-PVA-EC-LiCF₃SO₃ blend system irradiated with swift heavy O^{7+} ion beam.

In the present work we report the effect of irradiation with swift heavy O^{6+} ions on ionic conduction, dielectric relaxation and modulus formalism of Na⁺ cation in the blend of polymers PEO and PAM system.

2. Experimental details

Polyacrylamide (PAM; Molecular Weight = 50,00,000 gmol⁻¹) from Hi-Media, Polyethylene oxide (PEO; Molecular Weight = 300,000 gmol⁻¹) from Alfa Aesar and Sodium trifluoromethanesulfonate (NaCF₃SO₃) from Sigma Aldrich are obtained. All chemicals are used as received for preparing blend electrolyte samples. Concentration of salt has been taken by weight percentage varying as 5, 7.5, 10, 12.5, 15 and 17.5. Salt and both the polymers are dissolved in de-ionized water and stirred for 24 h in a magnetic stirrer. Homogeneous mixture is then transferred into teflon petri dish and allowed to dry. Free standing films of 160–220 μm thickness have been obtained after evaporating all traces of solvent at room temperature. The obtained films were stored in desiccator under vacuum for later use for measurement. FTIR spectra of all the samples are measured on a JASCO FTIR-4100 instrument in the wave number range of 1000–4000 cm⁻¹. SEM images are recorded on Hitachi SU 1510 instrument at a magnification of 2000X at 10 kV after gold coating on to the films by morphological detector at ambient temperature. For impedance measurement, Agilent E4980A Precision LCR meter instrument has been used in the frequency range of 20 Hz–2 MHz from ambient temperature to 333 K. The sample is placed between two blocking silver electrodes (dia. = 1.2 cm) under spring pressure for impedance measurements. Bulk electrolyte resistance and low frequency linear response are obtained from Nyquist plots by fitting to appropriate equivalent circuit.

For ion beam irradiation, free standing films are cut into 1 cm × 1 cm segments and mounted on the ladder maintaining a distance of 1 cm between all the samples. Irradiation with 80 MeV swift heavy O^{6+} ion beam is carried out using material science beam line facility of pelletron accelerator at IUAC, New Delhi. Irradiation has taken place at room temperature for four different fluences of 1×10^{11} , 3×10^{11} , 1×10^{12} and 2×10^{12} ions/cm² and a constant current of 0.4 pA (particle nano ampere) (flux) is maintained throughout the experiment.

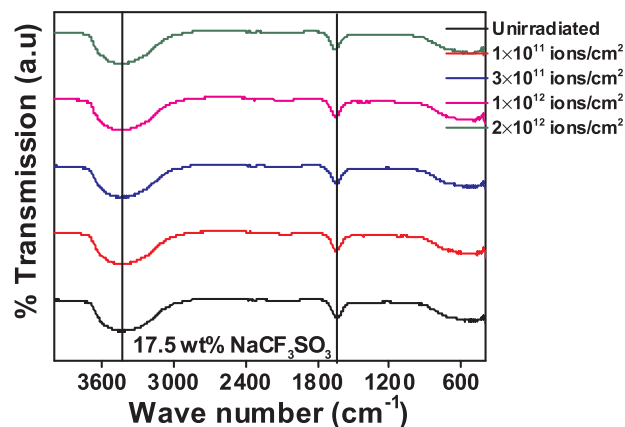


Fig. 1. FT-IR Spectra of un-irradiated and irradiated PEO-PAM-(17.5 wt%) NaCF₃SO₃ BPE sample.

3. Results and discussion

3.1. IR spectroscopy

Vibrational spectroscopy is extensively used for studying the modifications occurring in materials induced by ion beam irradiation and understanding the change in molecular bond lengths of the polymers or interaction between the constituents, if any. The IR spectra of the materials provide the information about the occurrence of complexation also between various constituents (Ramesh et al., 2007). Fig. 1 shows FT-IR spectra of sample with 17.5 wt% salt concentration un-irradiated and irradiated at various fluences. With increase in fluence from 1×10^{11} ions/cm² to 2×10^{12} ions/cm², only slight decrease in intensity of the peaks and minor shift towards higher wave-number side is observed. No extra peaks occur post irradiation. Irradiation degrades the polymer and breaking down of polymer chains results in changes in bond length and crystallinity which are manifested in the form of shifting of peaks and lowering of the intensity. These trivial changes observed in the IR-spectra of BPE samples, suggest that the irradiation definitely caused structural rearrangements, changes in bonds and isomerization (Kumar et al., 2010a, 2010b) in the electrolyte system but did not lead to a complete wipe-out of the overall structure of the polymer host matrix.

3.2. SEM studies

Fig. 2(a) to (e) show the SEM micrographs of pristine and irradiated samples for 5 wt% salt concentration at fluences 1×10^{11} ions/cm², 1×10^{12} ions/cm² and 2×10^{12} ions/cm². Fig. 2(a) shows a rough morphology with no remarkable sharp features in an un-irradiated sample. In Fig. 2(b) to (e), a gradual development of void like pores are observed from 1×10^{11} ions/cm²- 2×10^{12} ions/cm² fluence. Maximum pores are observed for 1×10^{12} ions/cm² fluence and at 2×10^{12} ions/cm² fluence, an obvious decrease in the pore structure is noted. When polymers are exposed to SHI irradiation, stiff chains of the polymers undergo scissioning due to its degradation. These broken chains form disordered pore-like structures with voids in between them are observed. At lower fluences, chain scissioning process dominates and very prominent pore structures are observed. At higher fluence, a large number of shattered chains recombine to form a rigid cross-linked network and an apparent decrease in the pore structures is noted. Seki et al. (2012) also observed significant surface modifications in the microstructure of carbon nanofibers post ion beam irradiation. A continuous change in SEM structure as a consequence of increase in disorderliness of the electrolytes, suggest an increase in amorphous nature of the system, enhancing with the increase of irradiation amount. The significant changes observed in electrolyte films confirm that

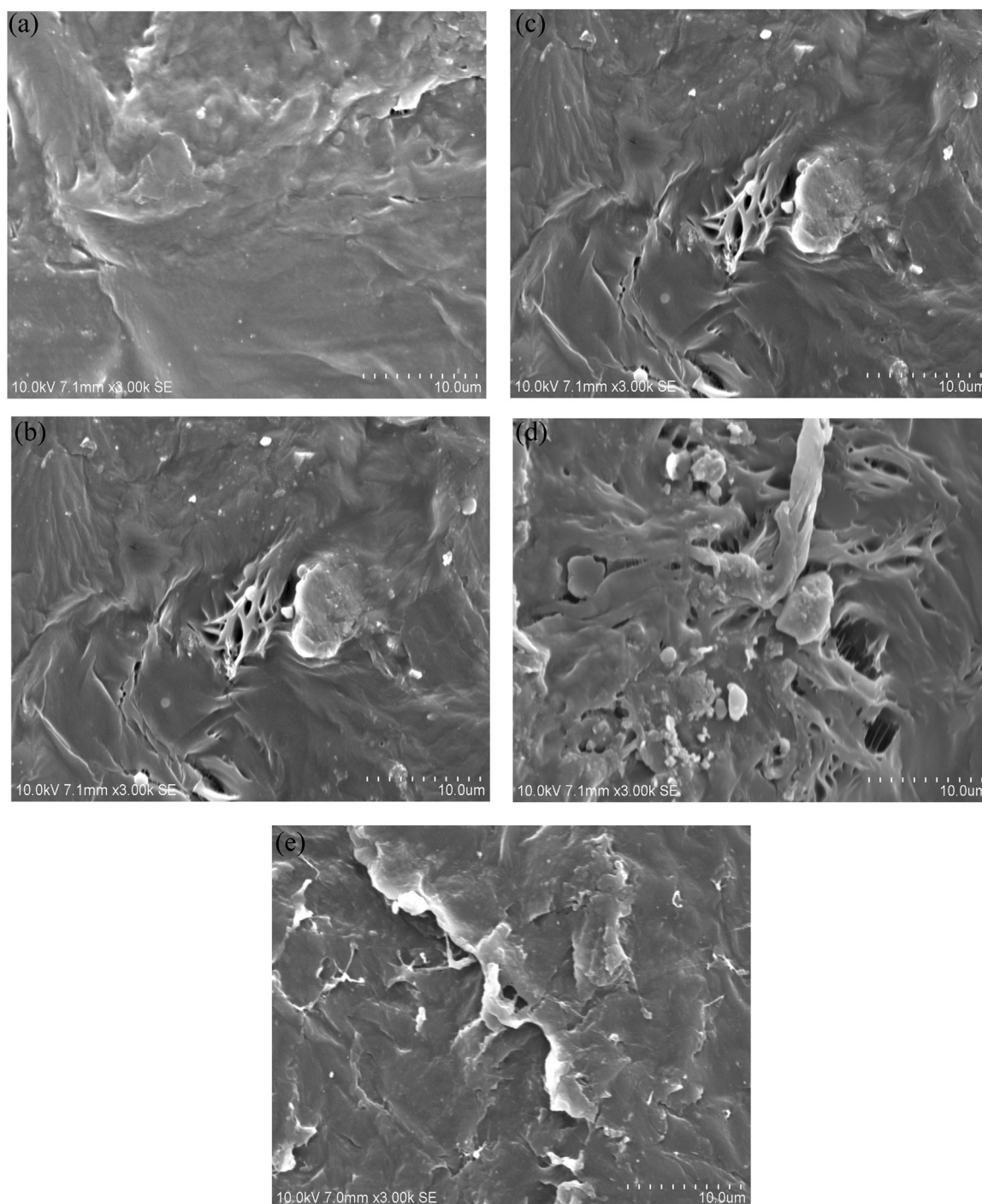


Fig. 2. (a) SEM Micrograph of un-irradiated electrolyte sample Fig. 2(b) SEM Micrograph of blend electrolyte sample irradiated at 1×10^{11} ions/cm² fluence. Fig. 2(c) SEM Micrograph of blend electrolyte sample irradiated at 3×10^{11} ions/cm² fluence. Fig. 2(d) SEM Micrograph of blend electrolyte sample irradiated at 1×10^{12} ions/cm² fluence. Fig. 2(e) SEM Micrograph of blend electrolyte sample irradiated at 2×10^{12} ions/cm² fluence.

irradiation by ion beam modifies the microstructure and such changes are dependent on fluence rate.

3.3. Ionic conductivity

Nyquist plots of un-irradiated and irradiated blend electrolyte sample with 17.5 wt% salt concentration at 323 K are plotted in Fig. 3. All samples show typical depressed semicircle (in the present case only the ending arc of the semicircle is observed due to frequency limitation of the instrument) in the high frequency region and spikes with angle

less than 90° in the low frequency range. High frequency semi-circular arc describes conduction process occurring aggregately in the system and low frequency spikes appear due to the electric double layer formation at electrode-electrolyte interphase (Liang et al., 2015). Intercept of semi-circular arc on low frequency side on x-axis gives the value of bulk resistance R_b of the samples, calculated by fitting the Nyquist plots to an equivalent circuit. The values of conductivity are calculated by Eq. (1) given as,

$$\sigma = \frac{l}{A} \times \frac{1}{R_b} \quad (1)$$

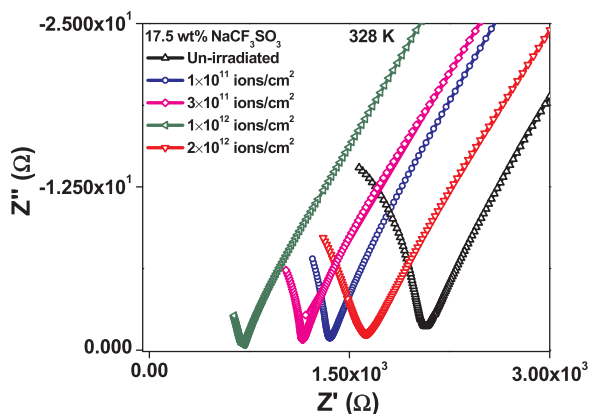


Fig. 3. Nyquist plots of un-irradiated and irradiated blend electrolyte samples with 17.5 wt% NaCF_3SO_3 at 328 K.

where, l is the thickness of the sample and A is the area of the electrodes used. Value of bulk resistance decreases with increase in fluence up to 1×10^{12} ions/cm² and then increases for fluence of 2×10^{12} ions/cm². When high energy ion beam travels through a polymer, the polymer chains flex and form microscopic disoriented segments. Breaking down of polymer chains weakens its microstructure and this contraction of the highly ordered system leads to decrease in crystallinity which is in conjunction with increase in amorphous phase of the system. Hence at lower fluences up to 1×10^{12} ions/cm², bulk resistance decreases. At 2×10^{12} ions/cm² fluence, substantial number of segments re-unite to form an augmented network structure leading to increase in value of R_b .

Fig. 4 shows conductivity as a function of fluence. Conductivity increases with successive dose up to 1×10^{12} ions/cm², and decreases at 2×10^{12} ions/cm² fluence. Maximum conductivity is 1.09×10^{-4} S/cm, recorded at 333 K for sample with 17.5 wt% salt, irradiated at 1×10^{12} ions/cm² fluence. The initial increase in conductivity can be due to the fact that at lower fluences, bonds in the polymer chains are broken (Saikia et al., 2006) and chain scission process dominates which leads to faster ionic transport through the polymer matrix assisted by larger segmental motion of the polymer backbone (Ismayil et al., 2015). According to Lee (1999), during irradiation, nuclear collisions may cause atomic displacements which lead to chain scission or discharge of pendant atoms. Polymers have a large free volume and hence the probability of displacing two atoms simultaneously from neighbouring chains and creating two radical pairs for cross-linking via nuclear collision is small. On the other hand, electronic excitations occur as a result of electromagnetic interactions between the positively charged ion and target nucleus. Hence, it produces a large number of free radicals,

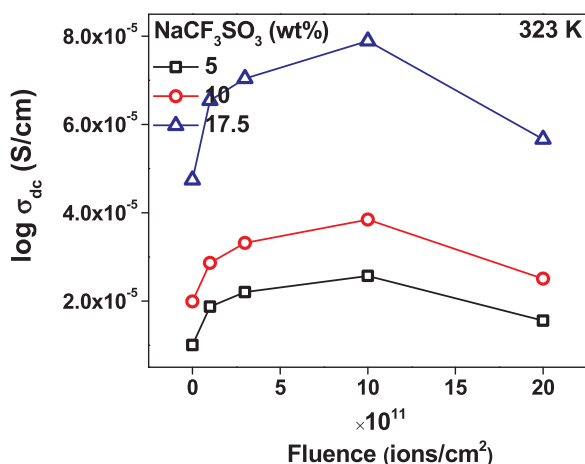


Fig. 4. Conductivity as a function of fluence.

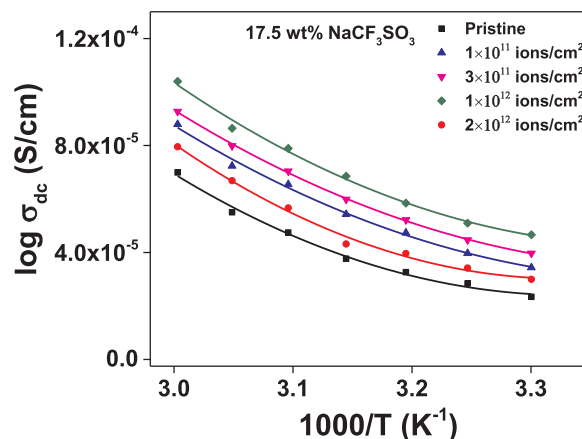


Fig. 5. Temperature response of conductivity of un-irradiated and irradiated BPE samples.

chemically active species, cations, anions and electrons along the ion track. Coulomb interactions among these active species cause rigorous bond stretching and segmental motion of polymer chains which leads to cross-linking and bond breaking. Hence both nuclear and electronic energy transfer, contribute to cross-linking and chain scissioning process. Nonetheless, nuclear stopping causes more chain scissioning because of its nature of independent damage, whereas in electronic stopping, a collective excitation takes place producing an excited volume within which coercive interactions among ions and the radicals occur leading to cross-linking of the polymer chains. Thus, at low fluence, chain scission predominates and at high fluence cross-linking mechanism takes charge. Activation energy required for cross-linking is provided by the critical fluence (10^{12} ions/cm² in the present case) above which re-crystallization of the system takes place and ionic conductivity reduces (Kumar et al., 2010a, 2010b).

3.3.1. Conductivity as a function of temperature

Conductivity response of un-irradiated and irradiated electrolyte samples with temperature is plotted in Fig. 5. The plot of $\log \sigma$ vs. $1000/T$ is evidently not a straight line according to Arrhenius relation, thus, the conductivity of polymer electrolyte are often best fitted by the empirical VTF.

The typical curvature behavior of the plots can be explained by VTF relation which indicates that the ion conduction strongly depends on polymer segmental motion. The VTF relation is given as follows.

$$\sigma = AT^{(-1/2)} \exp\left(-\frac{B}{K(T - T_0)}\right) \quad (2)$$

where A is pre-exponential factor, $B = E_h + E_j + \frac{w}{2z}$ is the apparent (Vogel) activation energy related to polymer segmental motion associated with the hybrid energy which considers the ionic jump E_j , dissociation energy $\frac{w}{2z}$ and energy of hole formation E_h (opposing internal and external pressure to produce a hole responsible for ionic transport), K is the Boltzmann constant, T_0 is the ideal glass transition temperature, i.e., the temperature at which the configuration entropy vanishes, typically taken to be 50 K below T_g (Nava et al., 2016; Lian et al., 2014; Itoh et al., 2013). Increase in temperature leads to faster polymer chain relaxation which produces segmental motion (Khair and Arof, 2007), leading to an increase in the free volume of the system. Increase in free volume, favours ion movement which results in increase in conductivity with temperature (Idris et al., 2007). During irradiation, the energy deposited in the polymer causes chain fracturing resulting in production of radicals which eventually decay or cross-link with neighbouring radicals. At low fluence, chain scission predominates because of skew radicals on different chains, which cannot crosslink due to their wide separation. On the other hand, as fluence increases, radical

Table 1
Activation Energy E_a values.

Fluence (ions/cm ²)	5% Salt	7.5% Salt	10% Salt	12.5% Salt	15% Salt	17.5% Salt
0	0.82	0.79	0.77	0.75	0.75	0.69
1×10^{11}	0.8	0.8	0.8	0.78	0.69	0.68
3×10^{11}	0.78	0.78	0.77	0.77	0.76	0.68
1×10^{12}	0.77	0.77	0.76	0.76	0.75	0.67
2×10^{12}	0.78	0.79	0.79	0.78	0.77	0.69

concentration increases resulting in formation of closely spaced radicals along the ion track. As a result coercive interaction among these radical pairs increases, which ultimately allows the adjacent polymer chains to cross-link (Kumar et al., 2010a, 2010b). Kumar et al. (2006) reported VTF behavior of Li^{3+} ion irradiated polymer electrolyte system and Saikia et al. (2006) noted VTF response of swift heavy ion irradiation effects on P(VDF–HFP) based gel polymer electrolytes. The VTF model proposes that ionic conductivity is favoured as a result of the segmental motion of polymer chains in the polymer matrix. The VTF relation is ensued over a wide range of temperature (303–333 K), which clearly indicates that a strong coupling exists between the ions of sodium trifluoromethanesulfonate salt and the polymer chain segments of the blend system of PEO and PAM.

Activation energy of an ionically conducting system is the minimum energy required by an ion to make a successful hop to participate in the conduction process. In Fig. 5, the solid lines are fits of the VTF equation to the σ , the solid lines are fits of the VTF equation to the σ_{ac} data. It is observed that the Vogel activation energy B marginally decreases as the fluence amount increases. Activation energy E_a , calculated from DC conductivity plots are presented in Table 1. Conductivity and activation energy as a function of fluence are plotted in Fig. 6. The plot shows that with increase in fluence, values of E_a decrease slightly and conductivity increases. The decrease in E_a with fluence is not quite significant though. Thus the increase in conductivity with temperature can be conveniently thought to occur due to increase in mobility of the ions after irradiation and not due to the increase in number of ions.

3.3.2. Frequency dependence of conductivity

Frequency dependent (AC) conductivity of the system for different fluences at 323 K is shown in Fig. 7. Three distinct regions are observed in the plots. Low frequency region is observed due to the electrode-electrolyte interface, the mid-frequency region is independent of frequency and is also called the DC region which is observed due to the diffusion of ions. Higher frequency region depicts the cross-over from DC region to AC region and the dominance of AC mechanism over DC

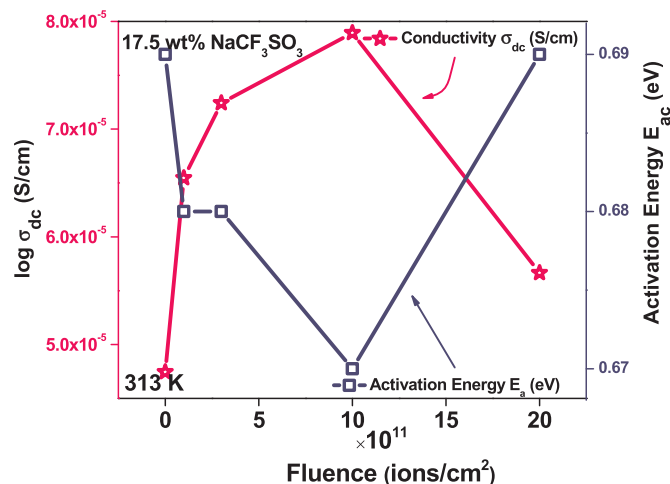


Fig. 6. Comparison of DC conductivity and Activation Energy according to Fluence.

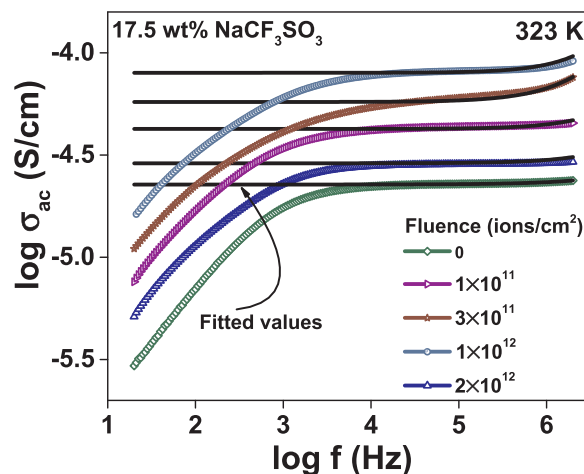


Fig. 7. Frequency dependent AC conductivity of un-irradiated and irradiated blend electrolyte samples.

(dispersion region). However, the third region becomes insignificant with increase in fluence and completely vanishes at critical fluence. The frequency region marked as (I) and (II) depict the dispersion frequency which is observed to shift towards higher frequency side with increase in fluence. This indicates that the relaxation times of the ions decrease and they hop more readily leading to an increase in conductivity with fluence.

Dispersive nature of conductivity with frequency can be well interpreted from Jonscher's Universal Power law (Jonscher, 1977).

$$\sigma(\omega) = \sigma_0 + A\omega^n \quad (3)$$

where $\sigma(\omega)$ is the value of AC conductivity, σ_0 depicts DC conductivity, A is a constant for particular temperature and n is the power law exponent related to degree of interaction amongst mobile ions and lattice around them (Jonscher, 1977; Pant et al., 2009).

3.4. Dielectric properties

3.4.1. Dielectric constant

Permittivity of dielectric materials is the measure the energy stored by them. Frequency dependent complex dielectric function ϵ^* of a material is given as (Sharma et al., 2013);

$$\epsilon^*(\omega) = \epsilon'(\omega) - i\epsilon''(\omega) = \frac{1}{i\omega C_0 Z^*} \quad (4)$$

Real and imaginary parts of complex impedance Z^* can be used to evaluate real and imaginary parts of the permittivity.

$$\epsilon' = \frac{-Z_i}{\omega C_0 (Z_r^2 + Z_i^2)} \quad (5)$$

$$\epsilon'' = \frac{-Z_r}{\omega C_0 (Z_r^2 + Z_i^2)} \quad (6)$$

where, C_0 is the capacitance of the material in vacuum, ϵ_0 is the permittivity of free space and has the value of $8.854 \times 10^{-12} \text{ F/m}$, $\omega = 2\pi f$ is the angular frequency and f is the frequency of the applied electric

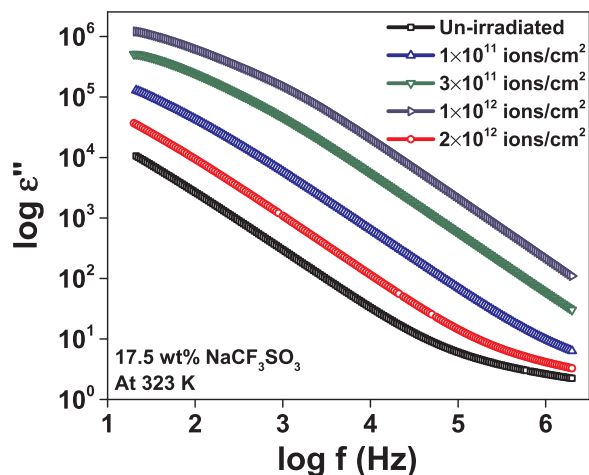


Fig. 8. Dielectric response of Un-irradiated and irradiated BPE sample.

field. Real part of permittivity ϵ' corresponds to ordinary dielectric constant of the material which measures the amount of elastic energy stored in the material during every cycle of applied alternating field and the energy responded back to the field at the end cycle.

Fig. 8 shows the dielectric behavior of the system before and after irradiation. Value of dielectric constant increases with increase in fluence from 1×10^{11} ions/cm² to 1×10^{12} ions/cm² and decreases at 2×10^{12} ions/cm² fluence. When a polymer material is subjected to irradiation by SHI, the processes of chain scissioning and cross-linking are triggered simultaneously in it. This leads to formation of defects such as bending and breaking of bonds, formation of new polar bonds and production of radicals (Lee, 1999). The fractured segments in polymer matrix act as dipoles which are oriented in the direction of the applied electric field. The irradiation of polymers increases the orientational polarization due to increase in number of dipoles with fluence (Kalia et al., 2018) which leads to increase in dielectric constant. As discussed in conductivity, chain scission process dominates at lower fluencies and hence more number of segments are available to participate in the orientational polarization process. At higher fluences (in the present case 2×10^{12} ions/cm²) cross-linking process takes over and hence the dielectric constant decreases due to decrease in number of segments effectively participating in the polarization process. Ismayil et al. (2015) have observed enhanced dielectric properties after γ -irradiation in PVA-NaBr composites. Bobby et al. (2016) have discussed the modifications induced by swift heavy C⁴⁺-ion irradiation on capacitance and dielectric properties of Ni/oxide/n-GaAs Schottky diode.

Dielectric constant shows high values at lower frequencies, gradually decrease with increase in frequency and reach a constant value at very high frequency. This is a general behavior of dielectric materials. Application of external electric field induces formation of dipoles in the dielectric materials which are polarized in the direction of the field. At lower frequencies, these dipoles are able to align themselves parallel to the field direction and hence the value of dielectric constant is higher. At higher frequencies, change in the electric field is very fast which the dipoles cannot follow and hence their contribution to polarization approaches a small value (Sharma et al., 2013). According to Gupta and Prajapati (2009), Correlated Barrier Hopping (CBH) model explains this phenomenon in terms of inter-well and intra-well hopping of the charge carriers. Average distance of inter-well hopping is few nm and that for intra-well hopping is of the order of one lattice spacing. At low frequency, the average relaxation time of the charge carriers is high and hence inter-well hopping mechanism is favoured which leads to increase in dielectric constant. Whereas, at higher frequencies, intra-well hopping is the governing mechanism because the charge carriers have barely enough time to move before which field reversal comes in and hence the dielectric constant decreases (Biju and Khadar, 2003).

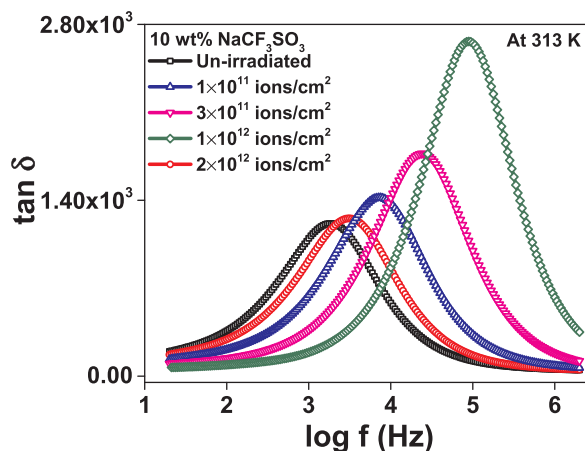


Fig. 9. Dielectric loss as a function of fluence.

3.4.2. Dielectric loss tangent

Dielectric loss spectra give the measure of energy loss occurring due to charge transport and electrode polarization effect. Fig. 9 shows dielectric loss response as a function of fluence. Dielectric loss peaks shift towards higher frequency side with increase in fluence. Occurrence of peak in loss spectra is a manifestation of dipolar relaxation phenomenon. On application of electric field to dielectric material, electrode polarization occurs due to deposition of charges, forming dipoles at the electrodes. These dipoles are forced to oscillate with the frequency same as that of the applied field and this gives rise to a relaxation phenomenon very similar to dipolar relaxation (Coelho, 1983). As observed from Fig. 9, the dielectric loss increases with increase in fluence up to 1×10^{12} ions/cm² and then decreases at 2×10^{12} ions/cm² fluence. Irradiation by SHI, accelerates formation of the dipoles contributing to dipolar relaxation and hence there is an increase in the loss with fluence. After a critical value of fluence (1×10^{12} ions/cm² in our case), formation of dipoles and thus the contribution to dielectric loss decreases. Ismayil et al. (2015) have reported significant increase in dielectric loss in PVA-NaBr polymer electrolyte system after γ -irradiation. Increase in dielectric loss was explained by Stevels (1957), to be a combination of conduction losses, dipole losses and vibrational losses. Conduction losses being proportional to (σ/ω) (where, σ is the conductivity and ω is the angular frequency) rise with rise influence as well as temperature which ultimately lead to increase in dielectric loss (Navratnam et al., 2015).

3.4.3. Modulus formalism

Electrode polarization at low frequency is a very pronounced effect and it subdues other relaxation processes (Karmakar and Ghosh, 2012). Modulus formalism has been exploited as one of the most powerful mechanisms to annex a wider insight into electrical relaxation processes occurring in frequency domain in various types of solids (Hodge et al., 2005).

Modulus formalism $M^*(f)$ can be well extracted from complex permittivity by the following relationships (Hodge et al., 2005; Macedo et al., 1972; McCrum et al., 1991; Dam et al., 2016).

$$M^*(\omega) = \frac{1}{\epsilon^*(\omega)} = M'(\omega) + jM''(\omega) \\ = M_\infty \left[1 - \int_0^\infty \exp(-j\omega t) \left(-\frac{d\phi(t)}{dt} \right) dt \right] \quad (7)$$

where, M' and M'' are the real and imaginary parts of the complex modulus M^* . The function $\phi(t)$ gives the time evolution of the electric field within the material and $\omega = 2\pi f$ is the angular frequency. Analysis of electrical relaxation in terms of complex permittivity $\epsilon^*(\omega)$ gives relaxation parameters, characteristics of the decay of the

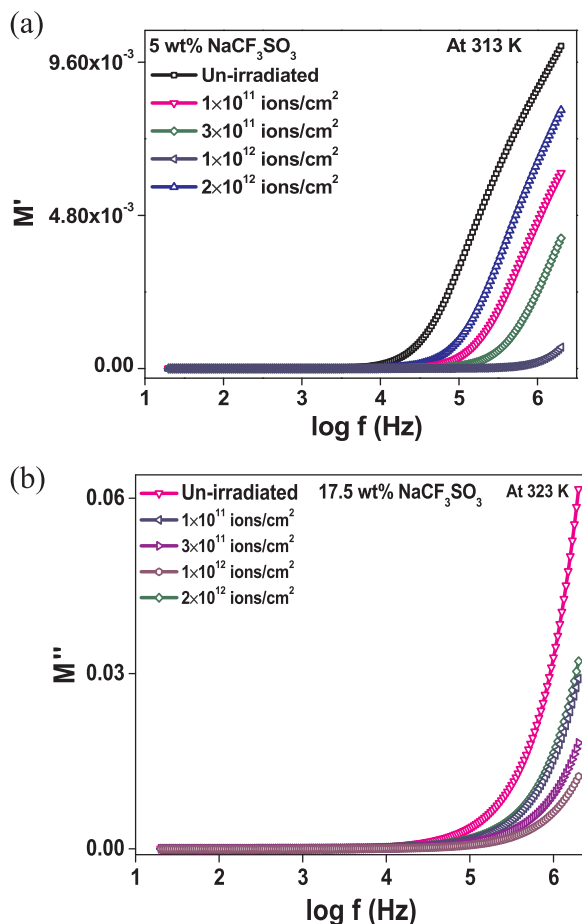


Fig. 10. (a) M' spectra of BPE sample before and after irradiation Fig. 10(b) M'' spectra of BPE sample before and after irradiation.

displacement vector \vec{D} . The expression for the decay of electric field in time domain can be written as

$$\vec{E}(t) = \vec{E}(0)\phi(t) \quad (8)$$

where $\vec{E}(0)$ denotes the electric field at time $t = 0$ and $\phi(t)$ is a macroscopic decay function of the general form

$$\phi(t) = \int_0^\infty g(\tau_\sigma) \exp[-(t/\tau_\sigma)^\beta] d\tau_\sigma \quad (9)$$

where τ_σ is conductivity relaxation time, and $g(\tau_\sigma)$ is a normalized density function for relaxation times. Thus using, Eqs. (8) and (10), it becomes

$$M^*(\omega) = M_\infty \int_0^\infty g(\tau_\sigma) \left[\frac{j\omega\tau_\sigma}{1+j\omega\tau_\sigma} \right] d\tau_\sigma \quad (10)$$

Fig. 10(a) and (b) show the modulus behavior of the system with fluence. Values of M' and M'' increase with increase in fluence. Relaxation peak is not observed for M' or M'' . In both cases there is a long tail appearing in the low frequency region is attributed to the large capacitance associated with the electrode polarization phenomenon (Pant et al., 2009). Due to limitation of frequency range of the instrument, relaxation peaks are not observed in the modulus spectra. Modulus behavior can, therefore, be interpreted as follows. With increase in fluence and temperature, the onset of the dispersion frequency of modulus spectra shifts towards higher frequency side. This suggests that the relaxation time decreases and it is related to the caged motion of the charge carriers (Marinov et al., 2017). At higher frequencies, the ions are not able to follow the field reversal and hence stay caged in the polymer matrix. The dispersion frequency shifts towards higher

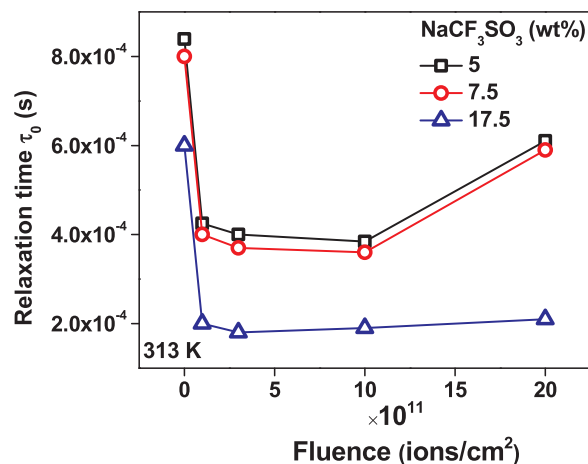


Fig. 11. Relaxation time as a function of fluence.

frequency side upto a fluence of 1×10^{12} ions/cm² and then shifts towards lower side at fluence of 2×10^{12} ions/cm². Raghu et al. (2014) explained that shifting in dispersion frequency with increase in fluence occurs due to the release of increased number of trapped charge carriers and their long distance hopping. Relaxation time $\tau_0 (= \frac{1}{\omega_{dis}})$ is calculated from the onset of dispersion phenomenon and presented in Fig. 11. It is observed that, the relaxation time decreases with increase in fluence upto 1×10^{12} ions/cm² and then increases for 2×10^{12} ions/cm². Decrease in relaxation time with increase in fluence denotes faster motion of ions and hence a higher conductivity of the irradiated samples.

4. Conclusion

Irradiation by swift heavy ion beam (SHI) studies on PEO-PAM-NaCF₃SO₃ blend polymer electrolyte system have shown changes in the morphological properties of the blend electrolyte system. IR spectra and SEM micrographs clearly depict such changes. Irradiation deforms the ordered chains of the polymer structure by chain scissioning process which is pronounced at lower fluence rates and manifests as increase in ionic conductivity and enhanced dielectric properties. Temperature dependence of conductivity shows VTF behavior before and after irradiation. The relaxation time of charge carriers decreases and conductivity increases with irradiation upto critical value of fluence equal to 1×10^{12} ions/cm². Beyond this, at a fluence of 2×10^{12} ions/cm², cross-linking of the polymer chains causes a decrease in amorphocity and in electrical properties.

Acknowledgements

Authors are thankful to IUAC, New Delhi for the award of Junior Research Fellowship under the grant No. BTR- 54319 and beam time at the accelerator Center.

References

- Armand, M.B., Chagabo, J.M., Duclot, M.J., 1979. In: Duclot, M.J., Vanishtha, P., Mundy, M., Shenoy, G.K. (Eds.), *Fast Ion Transport in Solids*. Amsterdam, North Holland., pp. 131.
- Abdul-Kader, A.M., El-Gandy, Y.A., Al-Rashdy, A.A., 2012. Improve the physical and chemical properties of biocompatible polymer material by MeV He ion beam. *Radiat. Phys. Chem.* 81, 798–802. <https://doi.org/10.1016/j.radphyschem.2012.04.009>.
- Bobby, A., Shiwakoti, N., Verma, S., Asokan, K., Antony, B.K., 2016. Frequency dependent negative capacitance effect and dielectric properties of swift heavy ion irradiated Ni/Oxide/n-GaAs Schottky diode. *Physica B.* 489, 23–27. <https://doi.org/10.1016/j.physb.2016.02.002>.
- Biju, V., Khadar, M.A., 2003. Dielectric properties of nanostructured nickel oxide. *J. Mater. Sci.* 38, 4055–4063. <https://doi.org/10.1023/A:1026131103898>.
- Chandra, A., Bhatt, A., Chandra, A., 2011. Ion transport properties of Hot-pressed Solid Polymer Electrolytes: (1-x)PEO: xNaHCO₃. *International Conference on Nanoscience,*

- Technology and Societal Implications. 10.1109/NSTSL.2011.6111776.
- Coelho, R., 1983. On the relaxation of a space charge. *Rev. Appl. Phys.* 18, 137–146. <https://doi.org/10.1051/rphysap:01983001803013700>.
- Dave, G., Kanchan, D.K., Singh, P., 2018. Conductivity studies of polymer electrolyte system irradiated with swift heavy O^{6+} ion beam. *AIP Conf. Proc.* 1941 (140087), 1–4. <https://doi.org/10.1063/1.5029218>.
- Delgado, A.O., Rizzuto, M.A., Tabacucis, M.H., Added, N., Fimk, D., 2009. Infrared analysis of ion beam irradiated polymers. *Nucl. Instrum. Methods Phys. Res. B* 267, 1546–1548. <https://doi.org/10.1016/j.nimb.2009.01.078>.
- Dam, T., Tripathy, S.N., Paluch, M., Jena, S.S., Pradhan, D.K., 2016. Investigations of relaxation dynamics and observation of nearly constant loss phenomena in PEO₂₀-LiCF₃SO₃-ZrO₂ based polymer nano-composite electrolyte. *Electrochim. Acta* 202, 147–156. <https://doi.org/10.1016/j.electacta.2016.03.134>.
- Gohel, K., Kanchan, D.K., 2018. Ionic conductivity and relaxation studies in PVDF-HFP: PMMA-based gel polymer blend electrolyte with LiClO₄ salt. *J. Adv. Dielectr.* 8 (185005), 1–13. <https://doi.org/10.1122/S2010135X18500054>.
- Gupta, P.N., Prajapati, G.K., 2009. Conduction mechanism in un-irradiated and γ -irradiated PVA-H₃PO₄ polymer electrolytes. *Nucl. Instrum. Methods Phys. Res. B* 267, 3328–3332. <https://doi.org/10.1016/j.nimb.2009.07.006>.
- Hema, M., Tamilselvi, P., 2016. Lithium ion conducting PVA:PVDF polymer electrolyte doped with nano SiO₂ and TiO₂ filler. *J. Phys. Chem. Solids* 96–97, 42–48. <https://doi.org/10.1016/j.jpcs.2016.04.008>.
- Hasa, I., Passerini, S., Hassoun, J., 2016. Characteristics of an ionic liquid electrolyte for sodium-ion batteries. *J. Power Sources* 303, 203–207. <https://doi.org/10.1016/j.jpowsour.2015.10.100>.
- Hodge, I.M., Ngai, K.L., Moynihan, C.T., 2005. Comments on the electric modulus function. *J. Non-Cryst. Solids* 351, 104–115. <https://doi.org/10.1016/j.jnoncrysol.2004.07.089>.
- Ismayil, Vasachar, R., Bhajantri, R.F., Dhola, P.S., Ganesh, S., 2015. Impact of electron beam irradiation on free volume related microstructural properties of PVA: NaBr polymer composites. *Nucl. Instrum. Methods Phys. Res. B* 342, 29–38. <https://doi.org/10.1016/j.nimb.2014.09.21>.
- Itoh, T., Fujita, K., Inoue, K., Iwama, H., Kondoh, K., Uno, T., Kubo, M., 2013. Solid Polymer electrolytes based on alternating copolymers of vinyl ethers with methoxy oligo(ethyleneoxy)ethyl groups and vinylene carbonate. *Electrochim. Acta* 112, 221–229. <https://doi.org/10.1016/j.electacta.2013.08.124>.
- Idris, N.H., Senin, H.B., Arof, A.K., 2007. Dielectric spectra of LiTFSI-doped chitosan/PEO blends. *Ionics* 13, 213–217. <https://doi.org/10.1007/811581-007-0093-z>.
- Joge, P., Kanchan, D.K., Sharma, P., Jayswal, M., Avasthi, D.K., 2014. Effect of swift heavy O⁷⁺ ion radiations on conductivity of lithium based polymer electrolyte. *Radiat. Phys. Chem.* 100, 74–79. <https://doi.org/10.1016/j.radphyschem.2014.03.025>.
- Jonscher, A.K., 1977. The ‘universal’ dielectric response. *Nature* 267, 673–679. <https://doi.org/10.1038/26767390>.
- Karmakar, A., Ghosh, A., 2012. Dielectric permittivity and electric modulus of polyethylene oxide (PEO)-LiClO₄ composite electrolytes. *Curr. Appl. Phys.* 12, 539–543. <https://doi.org/10.1016/j.cap.2011.08.017>.
- Kalia, R., Sharma, J.K., Kalia, S., 2018. Swift Heavy ion irradiation effects on dielectric loss in poly (ether ether ketone) (PEEK). *Adv. Mater. Proc.* 3, 146–150. <https://doi.org/10.5185/amp.2018/986>.
- Khair, A.S.A., Arof, A.K., 2007. Conductivity studies of starch-based polymer electrolytes. *Ionics* 16, 123–129. <https://doi.org/10.1007/s11581-009-0356-y>.
- Kim, S., Park, M.J., Balsara, N.P., Liu, G., Minor, A.G., 2011. Minimization of focused ion beam damage in nanostructured polymer thin films. *Ultramicroscopy* 111, 191–199. <https://doi.org/10.1016/j.ultramic.2010.11.027>.
- Kumar, A., Banerjee, S., Deka, M., 2010a. Electron microscopy for understanding swift heavy ion irradiation effects on electroactive polymers. In: Mendez-Vilaz, A., Diaz, J. (Eds.), *Microscopy: Science, Technology, Applications and Education*. Formatex Research Centre, Spain, pp. 1755–1768.
- Kumar, A., Deka, M., Banerjee, S., 2010b. Enhanced ionic conductivity in oxygen ion irradiated poly(vinylidene fluoride-hexafluoropropylene) based nanocomposite gel polymer electrolytes. *Solid State Ion.* 181, 609–615. <https://doi.org/10.1016/j.ssi.2010.02.027>.
- Kumar, A., Saikia, D., Singh, F., Avasthi, D.K., 2006. Li³⁺ ion irradiation effects on ionic conduction in P(VdF-HFP)-(PC+DEC)-LiClO₄ gel polymer electrolyte system. *Solid State Ion.* 177, 2575–2579. <https://doi.org/10.1016/j.ssi.2006.04.015>.
- Kumar, K.K., Ravi, M., Pavani, Y., Bhavani, S., Sharma, A.K., Narasimha Rao, V.V.R., 2011. Investigation on the effect of complexation of NaF salt with polymer blend (PEO/PVP) electrolytes on ionic conductivity and optical energy band gaps. *Phys. B: Condens. Matter* 406, 1706–1712. <https://doi.org/10.1016/j.physb.2011.02.010>.
- Lakshmi, G.B.V.S., Siddiqui, A.M., Ali, V., Kuriya, P., Zulfequar, M., 2008. Effects of 60 MeV C⁵⁺ ion irradiation on PmT-PVC and p-TSA doped PoT-PVC blends. *Nucl. Instrum. Methods Phys. Res. B* 266, 1685–1691. <https://doi.org/10.1016/j.nimb.2008.01.069>.
- Liang, B., Tang, S., Jiang, Q., Chen, C., Chen, X., Li, S., Yan, X., 2015. Preparation and characterization of PEO-PMMA polymer composite electrolytes doped with nano-Al₂O₃. *Electrochim. Acta* 169, 334–341. <https://doi.org/10.1016/j.electacta.2015.04.039>.
- Lee, E.H., 1999. Ion-beam modification of polymeric materials-fundamental principles and applications. *Nucl. Instrum. Methods Phys. Res. B* 151, 29–41. [https://doi.org/10.1016/S0168-583X\(99\)00129-9](https://doi.org/10.1016/S0168-583X(99)00129-9).
- Lian, F., Guan, H.-y., Wen, Y., Pan, X.-r., 2014. Polyvinyl formal based single-ion conductor membranes as polymer electrolytes for lithium ion batteries. *J. Membr. Sci.* 469, 67–72. <https://doi.org/10.1016/j.memsci.2014.05.065>.
- Macedo, P.B., Moynihan, C.T., Bose, R., 1972. The Role of Ionic Diffusion in Polarization in Vitreous Ionic Conductors. *Phys. Chem. Glass.* 13, 171–179.
- Marinov, Y.G., Hadjichristov, G.B., Petrov, A.G., Koduru, H.K., Marino, L., Scaramuzza, N., 2017. Dielectric and electrical behaviour of polymeric (PEO/PVP): NaO₄ composite for solid electrolytes. *IOP Conf. Ser.: J. Phys.* 794, 012020. <https://doi.org/10.1088/1742-6596/794/1/012020>.
- McCrum, N.G., Read, B.E., Williams, G., 1991. *An elastic and dielectric effects in polymeric solids*. Dover, New York.
- Monti, D., Ponrouch, A., Palacin, M.R., Johansson, P., 2016. Towards safer sodium-ion batteries via organic solvent/ionic liquid based hybrid electrolytes. *J. Power Sources* 324, 712–721. <https://doi.org/10.1016/j.jpowsour.2016.06.003>.
- Morena, J.S., Armand, M., Berman, M.B., Greenbaum, S.G., Scrosati, B., Panero, S., 2014. Composite PEO_n:NaTFSI polymer electrolyte: preparation, thermal and electrochemical characterization. *J. Power Sources* 284, 695–702. <https://doi.org/10.1016/j.jpowsour.2013.09.137>.
- Nanda, P., De, S.K., Manna, S., De, U., Tarafdar, S., 2010. Effect of gamma irradiation on a polymer electrolyte: variation in crystallinity, viscosity and ion-conductivity with dose. *Nucl. Instrum. Methods Phys. Res. B* 268, 73–78. <https://doi.org/10.1016/j.nimb.2009.09.063>.
- Nath, A.K., Kumar, A., 2010. Scaling of AC Conductivity, electrochemical and thermal properties of ionic liquid based polymer nanocomposite electrolytes. *Electrochim. Acta* 129, 177–186. <https://doi.org/10.1016/j.electacta.2014.02.101>.
- Nava, D.P., Guzmán, Vazquez-Arenas, J., Cardoso, J., Gomez, B., Gonzalez, I., 2016. An experimental and theoretical correlation to account for the effect of LiPF₆ concentration on the ionic conductivity of poly(poly(ethylene glycol) methacrylate). *Solid State Ion.* 290, 98–107. <https://doi.org/10.1016/j.ssi.2016.03.020>.
- Navratnam, S., Ramesh, K., Ramesh, S., Sanusi, A., Basirun, W.J., Arof, A.K., 2015. Transport mechanism studies of chitosan electrolyte systems. *Electrochim. Acta* 175, 68–73. <https://doi.org/10.1016/j.electacta.2015.01.087>.
- Ngai, K.S., Subramaniam, R., Ramesh, K., Juan, J.C., 2016. A review of polymer electrolytes: fundamental approaches and applications. *Ionics* 22, 1259–1279. <https://doi.org/10.1007/s11581-016-1756-4>.
- Nimah, Y.L., Cheng, M., Cheng, J.H., Rick, J., Hwang, B., 2015. Solid-state polymer nanocomposite electrolyte of TiO₂/PEO/NaClO₄ for sodium-ion batteries. *J. Power Sources* 278, 375–381. <https://doi.org/10.1016/j.jpowsour.2014.11.047>.
- Pitawala, H.M.J.C., Dissanayake, M.A.K.L., Seneviratne, A.A., 2007. Combined effect of A₂O₃ nano-fillers and EC plasticizer on ionic conductivity enhancement in solid polymer electrolyte (PEO)₉LiTf. *Solid State Ion.* 178, 885–888. <https://doi.org/10.1016/j.ssi.2007.04.008>.
- Papoutsaki, M. –V., Maris, T.G., Pappas, E., Papadakis, A.E., Damilakis, J., 2013. Dosimetric characteristics of a new polymer gel and their dependence on post-preparation and post-irradiation time: effect on X-ray beam profile measurements. *Phys. Media* 29, 453–460. <https://doi.org/10.1016/j.ejmp.2013.01.003>.
- Pant, M., Kanchan, D.K., Gondaliya, N., 2009. Transport properties and relaxation studies in BaO substituted Ag₂O-V₂O₅-TeO₂ glass system. *Mater. Chem. Phys.* 115, 98–104. <https://doi.org/10.1016/j.matchemphys.2008.11.047>.
- Raghu, S., Archana, K., Sharanappa, C., Ganesh, S., Devendrapa, H., 2016. Electron beam and gamma ray irradiated polymer electrolyte films: dielectric properties. *J. Radiat. Res. Appl. Sci.* 9, 117–124. <https://doi.org/10.1016/j.jrras.2015.10.007>.
- Raghu, S., Kilarkaje, S., Ganesh, S., Nagaraja, G.K., Devendrapa, H., 2014. Effect of electron beam irradiation on polymer electrolytes: change in morphology, crystallinity, dielectric constant and AC conductivity with dose. *Radiat. Phys. Chem.* 98, 124–131. <https://doi.org/10.1016/j.radphyschem.2014.01.024>.
- Ramesh, S., Leen, K.H., Kumantha, K., Arof, A.K., 2007. FTIR studies of PVC/PMMA blend based polymer electrolytes. *Spectrochim. Acta Part A: Mol. Biomol. Spectrosc.* 66, 1237–1242. <https://doi.org/10.1016/j.saa.2006.06.012>.
- Saikia, D., Kumar, A., Singh, F., Avasthi, D.K., 2006. Study of Li³⁺ ion irradiation effects in P(VdF-HFP) based gel polymer electrolytes for application in Li-ion battery. *J. Phys. D: Appl. Phys.* 39, 4208–4214. <https://doi.org/10.1088/0022-3727/39/19/013>.
- Sapri, M.N.Z.M., Ahmad, A.H., 2015. Conductivity and dielectric studies of pure and doped poly(ethylene oxide) (PEO) solid polymer electrolyte films. *J. Teknol. (Sci. Eng.)* 6, 47–51. <https://doi.org/10.11113/j.tv76.5510>.
- Seki, N., Arai, T., Suzuki, Y., Kawakami, H., 2012. Novel polyimide-based electrospun carbon nanofibers prepared using ion beam irradiation. *Polymer* 53, 2062–2067. <https://doi.org/10.1016/j.polymer.2012.03.026>.
- Sharma, P., Kanchan, D.K., Gondaliya, N., Pant, M., Jayswal, M., 2013a. Conductivity Relaxation in Ag⁺ ion conducting PEO-PMMA-PEG polymer blends. *Ionics* 19, 301–307. <https://doi.org/10.1007/s11581-012-0738-4>.
- Sharma, P., Kanchan, D.K., Gondaliya, N., 2013b. Effect of ethylene carbonate concentration on structural and electrical properties of PEO-PMMA polymer blends. *Ionics* 19, 777–785. <https://doi.org/10.1007/s11581-012-0797-6>.
- Stevens, J.M., 1957. In: Flügge, S. (Ed.), *Handbuch der Physik*. Springer, Berlin, pp. 350.
- Subramaniam, R., Lu, S.-C., 2011. Effect of lithium salt concentration on crystallinity of poly(vinylidene fluoride-do-hexafluoropropylene)-based solid polymer electrolytes. *J. Mol. Struct.* 994, 403–409. <https://doi.org/10.1016/j.molstruc.2011.03.065>.
- Vignaroban, K., Kushagra, R., Elango, A., Badami, P., Mellander, B.-E., Xu, X., Tucker, T.G., Nam, C., Kannan, A.M., 2016. Current trends and future challenges of electrolytes for sodium-ion batteries. *Int. J. Hydrog. Energy* 41, 2029–2846. <https://doi.org/10.1016/j.ijhydene.2015.12.090>.
- Vélez, J.F., Álvarez, L.V., del Río, C., Herradón, B., Mann, E., Morales, E., 2017. Imidazolium-based mono and dicationic liquid sodium polymer gel electrolytes. *Electrochim. Acta* 241, 517–525. <https://doi.org/10.1016/j.electacta.2017.04.096>.
- Wang, C., Yeh, Y., Wongthitharom, N., Wang, Y., Tseng, C., Lee, S., Chang, W.-S., Chang, J.-K., 2015a. Rechargeable Na/Na_{0.44}MnO₂ cells with ionic liquid electrolytes containing various sodium solute. *J. Power Sources* 274, 1016–1023. <https://doi.org/10.1016/j.jpowsour.2013.09.137>.
- Wang, X., Zhang, Y., Xu, Q., Xu, J., Wu, B., Gong, M., Chu, J., Xiong, S., 2015b. Low-cost quasi-solid DSSC assembled with PVDF-based gel electrolyte plasticized by PC-EC and electrodeposited Pt counter electrode. *J. Photochem. Photobiol. A: Chem.* 311, 112–117. <https://doi.org/10.1016/j.jphotochem.2015.06.023>.

Dielectric relaxation and modulus studies of PEO-PAM blend based sodium salt electrolyte system

G Dave & D K Kanchan*

Solid State Ionics & Glass Research Laboratory, Physics Department, Faculty of Science,
The M S University of Baroda, Vadodara 390 002, India

Received 21 November 2017; accepted 19 June 2018

Dielectric properties of solid polymer electrolyte having PEO-PAM blend matrix with sodium trifluoromethane sulfonate (NaCF_3SO_3) as ionic salt have been studied. The samples have been prepared by solution cast technique. X-ray diffraction analysis has been carried to understand the formation of blend, complexation and crystallinity of the polymer blend with the variation of salt amount. Complex impedance spectroscopy has been used to study ionic conductivity, dielectric relaxation and modulus formalism as a function of frequency at various temperatures. Scaling of M'' spectra has been carried out and it has been found that the dynamic relaxation processes occurring in the system are dependent on temperature as well as salt concentration. Highest conductivity at room temperature has been found to be 2.81×10^{-7} S/cm for sample with 17.5 wt% NaCF_3SO_3 .

Keywords: Blend polymer electrolyte, Sodium triflate, Dielectric relaxation, Modulus formalism

1 Introduction

Solid polymer electrolytes (SPE) have been studied continuously since more than two decades for their conceivable applications in electrochemical devices such as solid state batteries and super capacitors. Wright¹ reported high conductivity for alkali metal salt complexes with solid polymer electrolytes. High molecular weight PEO (polyethylene oxide) based polymer electrolytes have been materialized as the most suitable host matrix. Polymer blending has been realized as one of the most promising technique for reducing the crystalline phase of PEO and obtaining a host matrix with better properties. The amorphous region of the polymers is enhanced by polymer blending which results in overall good conductivity of the electrolyte system². Blends of PEO with other polymers have been reported³⁻⁷. PAM (polyacrylamide) is largely amorphous in nature and commonly used matrix for nano-composite hydrogels⁸. PAM and PEO are both water soluble neutral pH polymers and harmonious with different electrode and current collector materials⁹. Generally, if a blend of PEO:PAM-salt is prepared, it may contain pure PEO crystalline regions, salt rich crystalline regions and amorphous regions formed out of PEO:PAM-salt complexation. The polymer

crystalline regions exhibit limited free space between and along the polymeric chains and produce restricted segmental motion of the polymeric chains. On the other hand, the free space in the amorphous region contributes to the mobility of ions supported by segmental motion of the polymeric chains in electrolyte systems. Thus, transport of ions in PEO:PAM blend systems is expected to be easier due to enhanced amorphous content in the system controlling the ionic conductivity¹⁰.

Lithium salt¹¹⁻¹³ based polymer electrolytes have been extensively used in battery applications since a long time. Lithium based compounds are very hazardous and the limited sources of lithium metal are not enough^{14,15}. Studies on conducting property of Na place it as a potential alternative to Li salt^{10,16-19}. Sodium has very well established itself as a competent candidate as compared to other metal ion electrolytes due to its material abundance, low cost and environment friendly nature^{15,20-22}.

Understanding the electrochemical properties of blend of PAM with PEO and sodium triflate as a salt will make an interesting and a thought-provoking study. Therefore, in the present study, we have discussed the dielectric relaxation behavior and modulus formalism of sodium-ion in the blend of PEO and PAM polymers.

*Corresponding author (E-mail: dkkanchan.ssi@gmail.com)

2 Experimental

Polyacrylamide (PAM; molecular weight = 50,00,000 gmol^{-1}) from Hi-Media, polyethylene oxide (PEO; molecular weight = 300,000 gmol^{-1}) from Alfa Aesar and sodium trifluoromethanesulfonate (NaCF_3SO_3) from Sigma Aldrich are obtained. All chemicals are used as received. For preparing blend polymer electrolytes, both polymers PEO and PAM were taken in (1:1) ratio by weight. Concentration of the salt (C) is also taken in weight ratios of the total polymer system as 5, 7.5, 10, 12.5, 15 and 17.5. Polymers and the salt as a whole are dissolved in deionized water and stirred for 24 h continuously to achieve a homogeneous mixture. Solutions thus prepared with different amounts of salt are solution casted into Teflon petri dish. Free standing films of 160-220 μm thickness have been obtained after evaporating all traces of solvent at room temperature. The obtained films were stored in desiccator under vacuum for later use for measurement.

Considering an ideal mixture, approximate EO/Na ratio is calculated using the following equation²³:

$$C = \left[\frac{M_{\text{salt}}}{\rho_{\text{salt}}} + \frac{EO}{Na} \cdot \frac{M_{EO}}{\rho_{PEO}} \right]^{-1} \quad \dots (2)$$

where, M_{salt} and ρ_{salt} are the molecular weight (172 gmol^{-1}) and density (1.49 gcm^{-3}) of salt NaCF_3SO_3 respectively. M_{EO} is the molecular weight of EO unit (44 gmol^{-1}) and the density ρ_{PEO} is (1.1 gcm^{-3})^{23,24}. X-ray diffraction analysis has been carried using Rigaku Miniflex model diffractometer instrument at ambient temperature. For impedance measurement, SOLARTRON-1260 Impedance/Gain-Phase Analyzer instrument has been used in the frequency range of 32 MHz - 1 Hz from ambient temperature to 338 K. The sample is placed between two blocking silver electrodes (dia. = 1.2 cm) under spring pressure for impedance measurements.

3 Results and Discussion

3.1 XRD analysis

Structural properties of a material depicting its crystalline nature, amorphous volume and crystallite sizes are studied using the XRD analysis. Diffractograms of the pure polymers and blend of the polymers without salt are shown in Fig. 1 and patterns for solid electrolyte samples are shown in Fig. 2. Calculated values of FWHM, average crystallite size, average inter-chain separation and percentage of crystallinity are presented in Table 1.

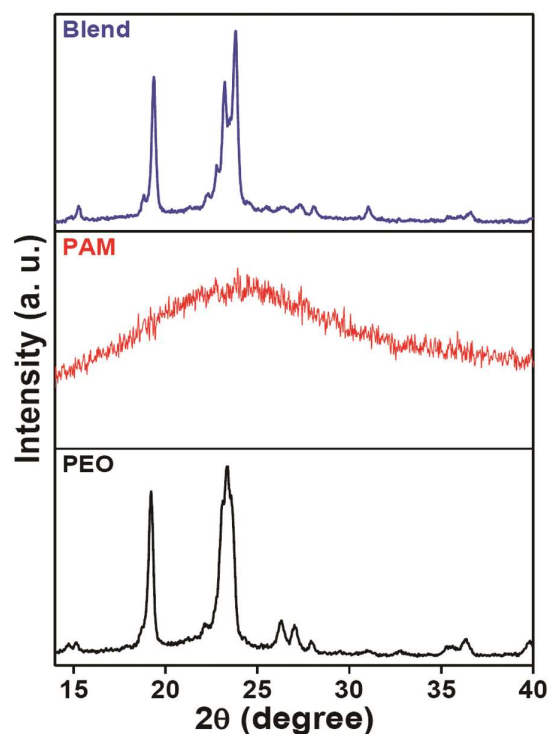


Fig. 1 – XRD patterns of pure PEO, PAM and blend sample without salt.

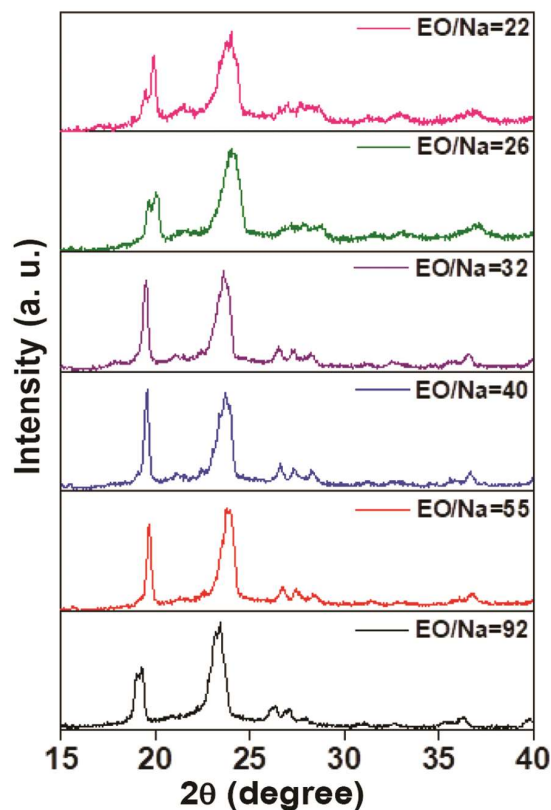


Fig. 2 – XRD spectra of electrolyte samples from EO/Na = 92 to EO/Na = 22.

Table 1 – XRD parameters and activation energies of pure PEO, pristine blend and blend electrolyte samples.

Sample	2θ (Degree)	FWHM β	L (nm)	R (Å)	% Crystallinity χ _c	Ionic conductivity (S/cm)	E _{ar} (eV)	E _{ac} (eV)
Pure PEO	19.22	0.32	0.4588	0.2824	67.30		-	-
	23.05	0.78	0.1931	0.2389				
Pristine Blend	19.47	0.39	0.3770	0.2868	62.13		-	-
	23.68	0.81	0.1869	0.2395				
EO/Na = 92	19.51	0.45	0.3268	0.2883	60.18	0.48×10 ⁻⁷	0.80	0.77
	23.70	0.93	0.1628	0.2398				
EO/Na = 55	19.51	0.54	0.2728	0.2888	58.23	0.63×10 ⁻⁷	0.79	0.79
	23.81	1.12	0.1357	0.2405				
EO/Na = 40	19.61	0.56	0.2624	0.2923	58.02	1.42×10 ⁻⁷	0.82	0.82
	23.92	1.25	0.1250	0.2425				
EO/Na = 32	19.79	0.60	0.2445	0.2944	56.30	1.47×10 ⁻⁷	0.79	0.79
	23.97	1.31	0.1109	0.2443				
EO/Na = 26	19.82	0.74	0.1991	0.2976	52.19	1.90×10 ⁻⁷	0.77	0.75
	24.02	1.40	0.1084	0.2465				
EO/Na = 22	19.93	0.81	0.1828	0.2984	48.72	2.81×10 ⁻⁷	0.70	0.69
	24.11	1.47	0.1030	0.2485				

Average crystallite size (L) is calculated using the Scherrer formula^{25,26}:

$$L = \frac{k\lambda}{\beta \cos\theta} \quad \dots (2)$$

where, β is the FWHM of the peak (in radian), k is the shape factor whose value is assumed to be 0.9 for calculating the parameters and λ is the wavelength of Cu-K_α line = 0.154056 nm.

The average inter-chain separation is calculated using the following equation²⁷:

$$R = \frac{5}{8} \frac{\lambda}{\sin\theta} \quad \dots (3)$$

The % crystallinity of the samples is calculated using the formula²⁸:

$$\chi_c = \frac{A}{A_0} \times 100 \quad \dots (4)$$

where, A is sum of areas of all crystalline peaks and A_0 is total area under entire diffractogram.

XRD patterns of pure polymers PEO, PAM and blend sample without salt are shown in Fig. 1. PAM shows only a broad hump at 2θ=25° indicating its amorphous nature. PEO shows crystalline peaks at 2θ=19° and 23° originating due to the orderings of poly ether side chains²⁹. In the blend sample without salt, characteristic peaks of PEO at 2θ=19° and 23° are observed and no hump is seen due to PAM in the blend spectra.

Figure 2 shows diffractograms of blend electrolyte samples with varying EO/Na ratio. At 2θ=19° and

23°, slightly broadened but intense peaks, as seen in pure PEO spectra, are observed in all the electrolyte samples. As the salt is added, the intensity of peak at 19° gradually increases up to EO/Na = 40 and then after it starts decreasing and the width also increases. The X-ray peak at 19° splits and broadens for EO/Na = 32 and beyond, while at 23°, the peaks broaden. Small peaks beyond 25° are observed to be broadened for the electrolyte films. Peaks corresponding to NaCF₃SO₃ are not observed in the electrolyte samples which ascertain that the salt does not remain as an individual entity in the system. Overall alteration in the diffractogram patterns of pristine components, suppression of peaks and decrease in intensities and non-occurrence of salt peaks in the electrolyte system suggest structural reorganization of polymers and complete dissociation of salt in the system at the molecular level resulting in a good polymer-polymer and polymer-salt complexation³⁰. From the above observations we can say that there is productive interaction amongst the constituent polymers which results in a miscible blend with traces of crystalline PEO.

Table 1 shows the values of various XRD parameters. Average crystallite size L and % crystallinity decrease with increase in salt concentration. Both the parameters indicate decrease in crystallinity with corresponding increase in amorphicity. Values of inter-chain separation R also increase with increase in salt content this leads to

increase in free volume of the system. Increase in free volume paves an easy conduction passage for mobile ion species leading to enhanced conductivity of the electrolyte system.

Apparent observations lead us to confirm the formation of a miscible blend electrolyte system which becomes more amorphous by successive addition of salt.

3.2 Ionic conductivity

Ionic conductivity of the blend electrolyte system was determined from complex impedance studies. Figure 3 shows Nyquist plots for the electrolyte samples at different concentrations of NaCF₃SO₃. Depressed semicircle in high frequency region and low frequency spikes with angle less than 90° are observed for all the samples. Intercept of semicircle on X-axis gives bulk resistance of the sample R_b. Then DC conductivity is found using the formula:

$$\sigma = \frac{1}{R_b} \times \frac{t}{A} \quad \dots (5)$$

where, *t* is the thickness of the sample and *A* is the area of the blocking electrodes. As observed from the plots, value of R_b decreases with increase in salt concentration. This suggests that the conductivity of the electrolyte system increases with increasing salt. Calculated values of conductivity are presented in Table 1.

Figure 4 shows variation of conductivity as a function of frequency at various NaCF₃SO₃ concentrations. Three distinct regions are observed in the plots for all the electrolyte samples. Low frequency region is observed due to polarization at the electrode-electrolyte interface and mid frequency

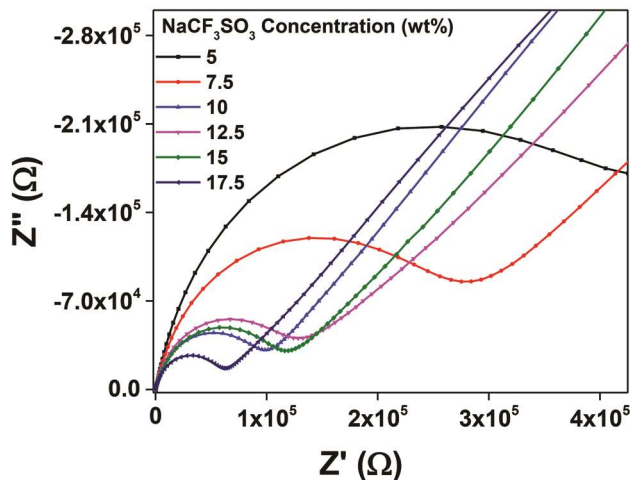


Fig. 3 – Nyquist plots for the electrolyte samples at different concentrations of NaCF₃SO₃.

region is independent of frequency and is also called DC region observed due to diffusion of ions. In this frequency range, ions travel much faster and jump from one site to another available site. Successful hopping of ions to a neighboring vacant site contributes to the DC conductivity, when the frequency is lower than the hopping frequency (ω_p). In the third region, i.e., the high frequency region, the frequency exceeds hopping frequency (ω_p) and the conductivity continues to increase with increase in frequency. The crossover from frequency independent conductivity to dispersion depicts the relaxation phenomenon. Variation of hopping frequency can be interpreted in terms of charge carriers as:

$$\omega_p = \left(\frac{\sigma_{DC}}{A} \right)^{1/n} \quad \dots (6)$$

where, σ_{DC} is DC conductivity of the sample, *A* is a constant for particular temperature and *n* is the power law exponent related to degree of interaction amongst mobile ions and lattice around them^{31,32}. The values of conduction activation energy *E_{ac}* are calculated from the values of ω_p and given in Table 1.

3.3 Dielectric studies

Permittivity of dielectric materials is the property used to measure the energy stored by them. Frequency dependent complex dielectric function ϵ^* of a material is given as³³:

$$\epsilon^*(\omega) = \epsilon'(\omega) - i\epsilon''(\omega) = \frac{1}{i\omega\epsilon_0 Z^*} \quad \dots (7)$$

Real and imaginary parts of complex impedance *Z** can be used to evaluate real and imaginary parts of the permittivity.

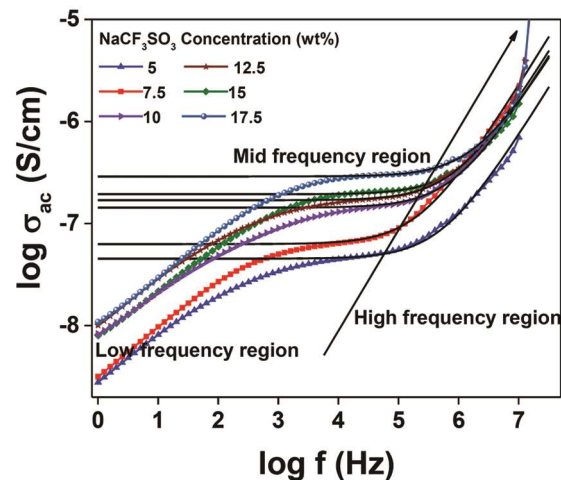


Fig. 4 – Variation of conductivity as a function of frequency at various NaCF₃SO₃ concentrations.

$$\epsilon' = \frac{-Z_i}{\omega C_0(Z_r^2 + Z_i^2)} \quad \dots (8)$$

$$\epsilon'' = \frac{-Z_r}{\omega C_0(Z_r^2 + Z_i^2)} \quad \dots (9)$$

where, C_0 is the capacitance of the material in vacuum, ϵ_0 is the permittivity of free space and has the value of $8.854 \times 10^{-12} \text{ F/m}$, $\omega = 2\pi f$ is the angular frequency and f is the frequency of the applied electric field. Real part of permittivity ϵ' corresponds to ordinary dielectric constant of the material which measures the amount of elastic energy stored in the material during every cycle of applied alternating field and the energy responded back to the field at the end cycle. Higher value of ϵ' suggests better conductivity. Figures 5 and 6, respectively, show frequency dependent ϵ' and ϵ'' at 323 K for different concentrations of NaCF_3SO_3 .

Sharp increase in ϵ' and ϵ'' at lower frequencies is observed due to the electrode polarization and space charge effects, which connote non-Debye behavior of the system³⁴. The higher value of dielectric loss (ϵ'') at low frequency is observed due to the long distance charge motion within the materials. The appearance of peak is attributed to the relaxation phenomena of polymer. In low frequency region, dipoles are able to align themselves according to the electric field direction and hence contribute in the polarization process. At high frequencies both dielectric constant ϵ' and ϵ'' approach almost constant value. As the frequency is increased, the change in electric field becomes too fast for the charges to follow and hence, because of internal frictional forces, their contribution

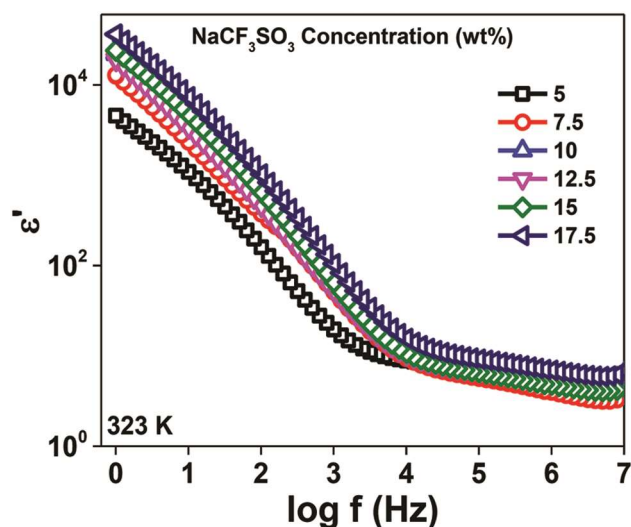


Fig. 5 – Frequency versus ϵ' plots with different salt concentration at 323 K.

to the polarization approaches a small value³³. As seen from Figs 5 and 6, the value of dielectric constant increases with increase in salt concentration and it is attributed to the increase in number of charge carriers with increasing amount of salt.

Figures 7 and 8, respectively, show frequency dependent ϵ' and ϵ'' plots for sample with 17.5 wt% NaCF_3SO_3 at different temperatures. The value of dielectric constant increases with increase in temperature. Applied electric field leads to formation of an electric moment inside the dielectric as a whole and also in each separate polarized molecule. These molecular dipoles cannot orient themselves at lower temperatures, increase in temperature favours the orientation of the dipoles and hence the value of dielectric constant increases³⁵.

3.4 Dielectric loss

Energy dissipation arising from charge transport and electrode polarization effect can be measured from dielectric loss. Electrode polarization occurs due to deposition of charges forming dipoles at the electrodes, which when applied by an electric field is forced to oscillate with the same frequency as that of applied field which leads to relaxation behavior similar to dipolar relaxation³⁶. According to this convention, the deposited charges show a relaxation peak in dielectric loss spectra. Stevels³⁷, explained increase in dielectric loss as the relaxation phenomenon due to conduction losses, dipole losses and vibrational losses. Conduction losses rise with increase in temperature, which in turn causes the

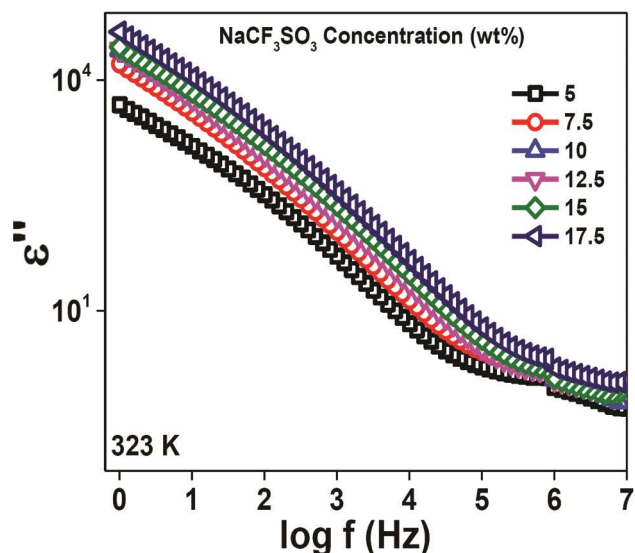


Fig. 6 – Frequency versus ϵ'' plots with different salt concentrations at 323 K.

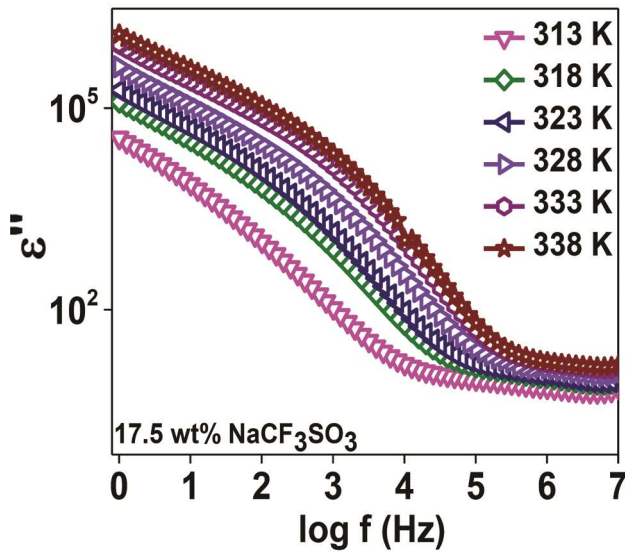


Fig. 7 – Frequency versus ϵ' plots for sample with 17.5 wt% salt at different temperatures.

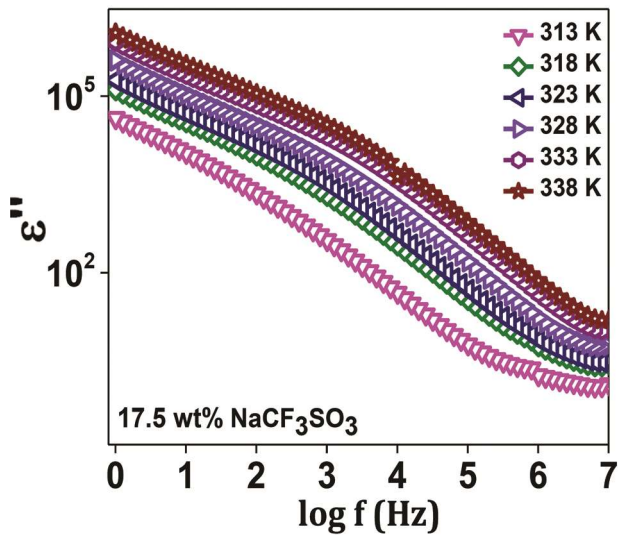


Fig. 8 – Frequency versus ϵ' plots for sample with 17.5 wt% salt at different temperatures.

value of dielectric loss to increase because conduction losses are proportional to (σ/ω) . The $\tan \delta$ peaks shift towards higher frequency side with successive addition of salt, i.e., relaxation time decreases. Figure 10 shows behavior of dielectric loss at various temperatures for sample with 17.5 wt% salt. From the plots, it is clear that $\tan \delta$ value increases with frequency at different temperatures, passes through a maximum value and thereafter decreases and is attributed to ion jump and dc conduction loss of ions accompanied with polarization losses. Figure 10 shows that the frequency for relaxation peaks

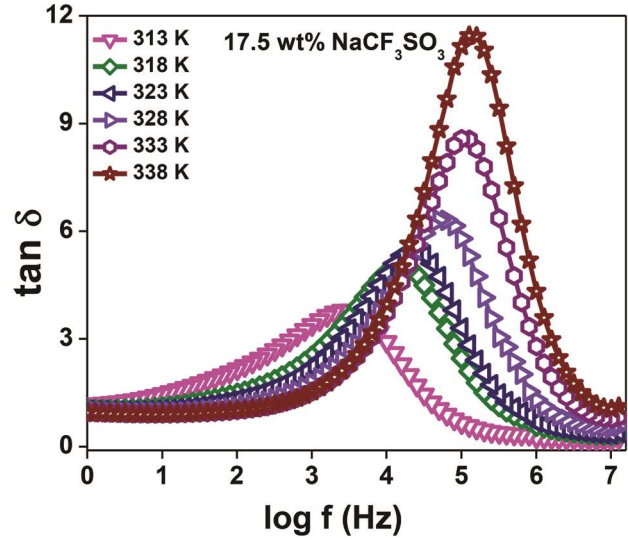


Fig. 9 – Frequency versus loss tangent at various salt concentrations.

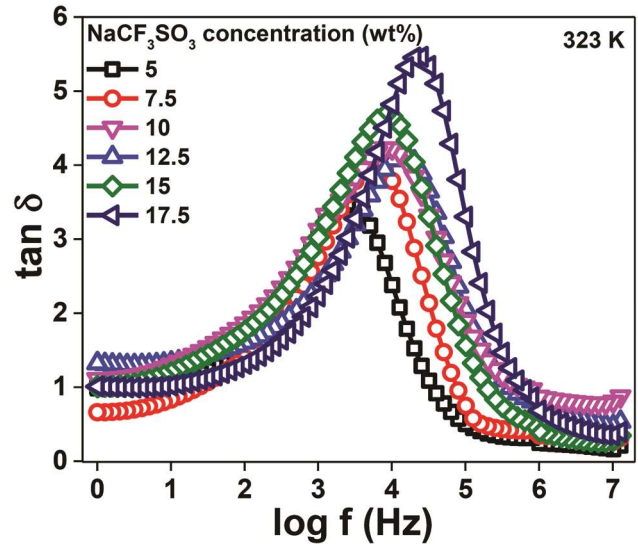


Fig. 10 – Frequency versus loss tangent for sample with 17.5 wt% salt at different temperatures.

increases with temperature and hence relaxation time decreases with increase in temperature. The decrease in relaxation time with increasing temperature is due to faster movement of sodium ions that synchronizes with the direction of applied field³⁰.

With increase in the salt concentration (Fig. 9), the magnitude of the loss increases and the loss peak shifts towards higher frequency side. The asymmetric shape of the ($\tan \delta$) peak around the maximum frequency (ω_{max}) suggests a deviation from classical exponential Debye behavior. The observed full width half maxima (FWHM) values of the $\tan \delta$ peaks are found to be broader than the ideal Debye peak. The

relaxation time, $\tau = 1/2\pi f_{max}$ can be calculated from the angular frequency ω_{max} at which the ($\tan\delta$) occurs. It is observed that the relaxation time decreases with increase in temperature as well as with the addition of sodium triflate.

3.5 Modulus studies

The dispersion behavior of the conductivity in the frequency domain is more conveniently interpreted in terms of conductivity relaxation time, τ using the electrical modulus, $M^* = 1/\epsilon^*$ representation. Complex electric modulus M^* formalism is used very frequently when the relaxation behavior is presumed to be due to the motion of ions or electrons. Further information about the relaxation behavior of any electrolyte can be obtained from the complex electric modulus $M^*(f)$. The conductivity behavior can be conveniently interpreted in terms of conductivity relaxation time, τ in the frequency domain. Ionic conductivity is described by the modulus representation by associating a conductivity relaxation time with the ionic process.

Dielectric relaxation is due to the re-orientation process of dipoles in the polymer chains, which culminates into a peak in M'' spectra. The real (M') and imaginary (M'') parts of $M^*(f)$ are calculated from the impedance data. Electric modulus is the electric counterpart of mechanical shear modulus; it corresponds to relaxation of electric field occurring at constant electric displacement³⁸. Modulus studies are carried out to interpret the electrical relaxation processes occurring in the material which are difficult to distinguish from the polarization effect occurring at electrode-electrolyte interface. Macedo³⁹, presented the study of dielectric modulus to overcome this drawback. McCrum and others⁴⁰ in their book on polymeric solids have also suggested the use of modulus formalism. Ever since its discovery, modulus function has been used by researchers worldwide to understand and explain electrical relaxation phenomenon in different types of materials⁴¹. A comparison of the experimental data of M^* and ϵ^* is, therefore, useful to distinguish long-range conduction process from the localized dielectric relaxation. The dielectric response of modulus formalism M^* of a system is treated with complex permittivity ϵ^* by the following relationship³⁹⁻⁴²:

$$M^*(\omega) = \frac{1}{\epsilon^*(\omega)} = M'(\omega) + jM''(\omega) \\ = M_\infty \left[1 - \int_0^\infty \exp(-j\omega t) \left(-\frac{d\phi(t)}{dt} \right) dt \right] \dots (10)$$

where M' and M'' are the real and imaginary parts of the complex modulus M^* . The function $\phi(t)$ gives the time evolution of the electric field within the material and $\omega = 2\pi f$ is the angular frequency.

Analysis of electrical relaxation in terms of complex permittivity $\epsilon^*(\omega)$ gives relaxational parameters, characteristics of the decay of the displacement vector \vec{D} . The expression for the decay of electric field in time domain can be written as:

$$\vec{E}(t) = \vec{E}(0)\phi(t) \dots (11)$$

where $\vec{E}(0)$ denotes the electric field at time $t=0$ and $\phi(t)$ is a macroscopic decay function of the general form:

$$\phi(t) = \int_0^\infty g(\tau_\sigma) \exp\left[-(t/\tau_\sigma)^\beta\right] d\tau_\sigma \dots (12)$$

where τ_σ is conductivity relaxation time, and $g(\tau_\sigma)$ is a normalized density function for relaxation times. Thus, using Eqs 10 and 12, it becomes:

$$M^*(\omega) = M_\infty \int_0^\infty g(\tau_\sigma) \left[\frac{j\omega\tau_\sigma}{(1+j\omega\tau_\sigma)} \right] d\tau_\sigma \dots (13)$$

Occurrence or absence of peak in frequency versus imaginary impedance plots is associated with space charge effects and non-localized conductivity. M' plots prove to be useful in understanding the behavior of the system when the relaxation processes are speculated to occur due to ionic motion and the electrode effects are suppressed. The plots of Z'' and M'' as a function of frequency, Fig. 11(a) clearly show that the Z'' peak is developed at low frequency side while the peak for M'' is observed at higher frequency for 5wt% salt concentration. The Z'' peak shifts towards higher frequency side and reverse mechanism occurs for M'' spectra peak with the addition of sodium triflate in the blend as observed in Fig 11(b). Thus, it can be ascribed that the shift in peak frequency of M'' spectra suggests slower ionic motion in the system with the addition of salt. Z'' and M'' peaks do not appear at the same frequency which shows that the relaxation times are disseminated and the system shows non-Debye behavior³³. Values of relaxation activation energy E_{ar} are calculated from the values of peak maxima of M'' spectra and presented in Table 1. It is noted from Table 1 that the values of conduction activation energies (E_{ac}) and relaxation activation energies (E_{ar}) are nearly same, this

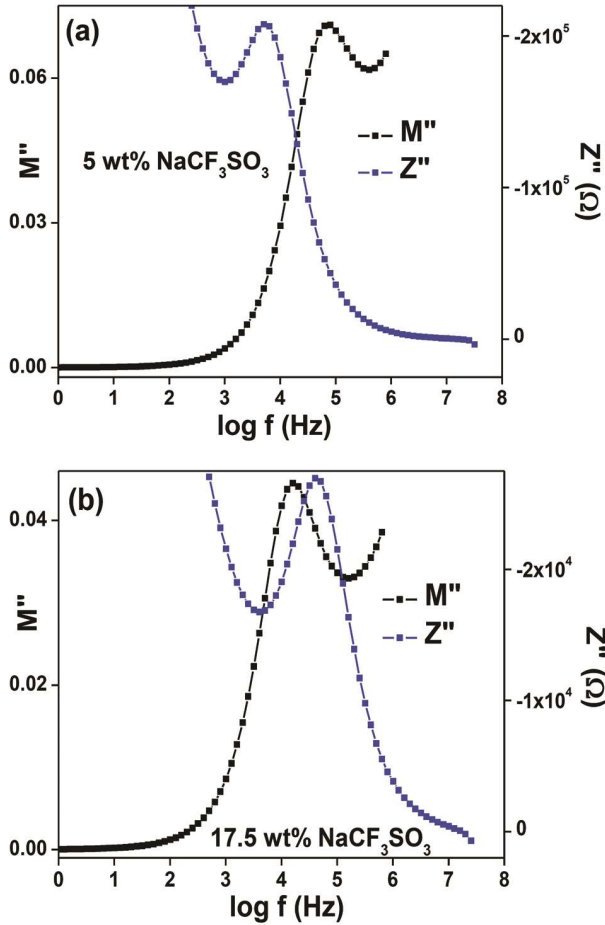


Fig. 11 – (a) Comparison of Z'' and M'' spectra of samples with 5 wt% salt concentration and (b) comparison of Z'' and M'' spectra of samples 17.5 wt% salt concentration.

suggests that the hopping mechanism dominates ion transport process in the present system and the ions encounter with equivalent barrier while relaxation and conduction processes⁴³. This shows that the ionic and polymer segmental motion are strongly coupled.

Figures 12 and 13 show the modulus behavior of the system with frequency. Values of M' increase with increase in frequency and attain maximum value in higher frequency range. M'' spectra show relaxation peak, which confirms the ionic nature of the material under study. The peak represents conductivity relaxation of the sodium ions in the system. Lower frequency side of the peak suggests long distance mobility of the charge carriers and the higher frequency side of the peak corresponds to caged movement of mobile ions²⁰. The long tail appearing in the low frequency region is attributed to the large capacitance associated with the electrode polarization phenomenon³². Plots of M' and M'' with frequency for

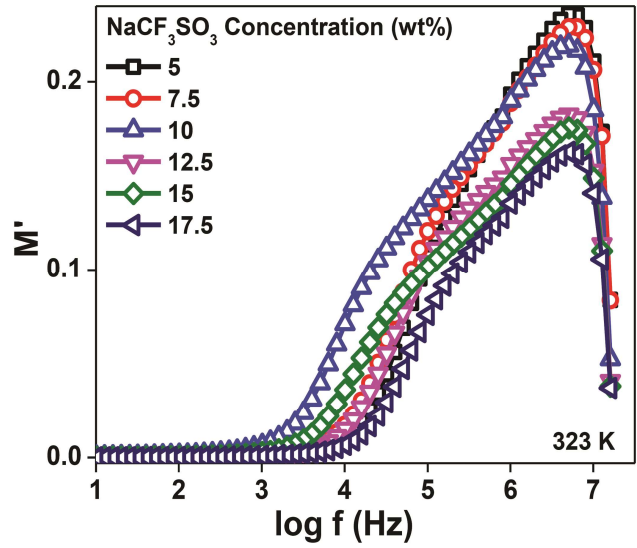


Fig. 12 – Frequency versus M' plots with salt concentration at 323 K.

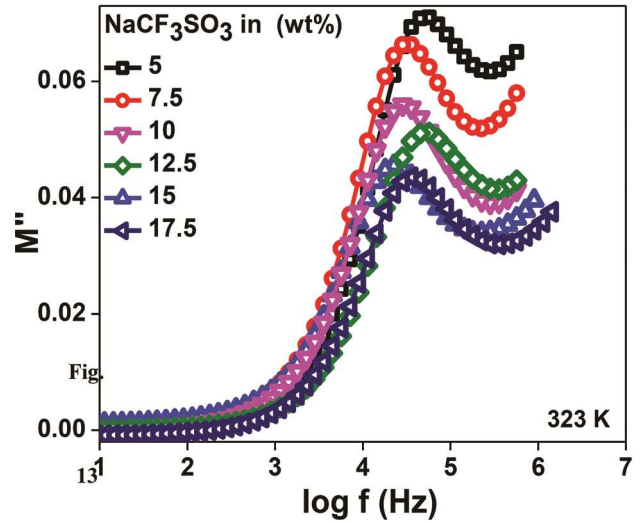


Fig. 13 – Frequency versus M'' plots with salt concentration at 323 K.

sample with 17.5 wt% salt concentration at various temperatures are shown in Figs 14 and 15. It is observed that M'' plots display distinct relaxation peaks, which are related to the conductivity processes. The relaxation time decreases at higher temperatures due to faster ionic motion, hence the peaks shift towards higher frequency side⁴³.

The decay function $\phi(t)$ (in Eq. (12)) exhibits non exponential in amorphous systems i.e., if there is a distribution of relaxation times. In time domain, the decay function is called stretched exponential introduced by Kohlraush-Williams-Watts (KWW) and is given as:

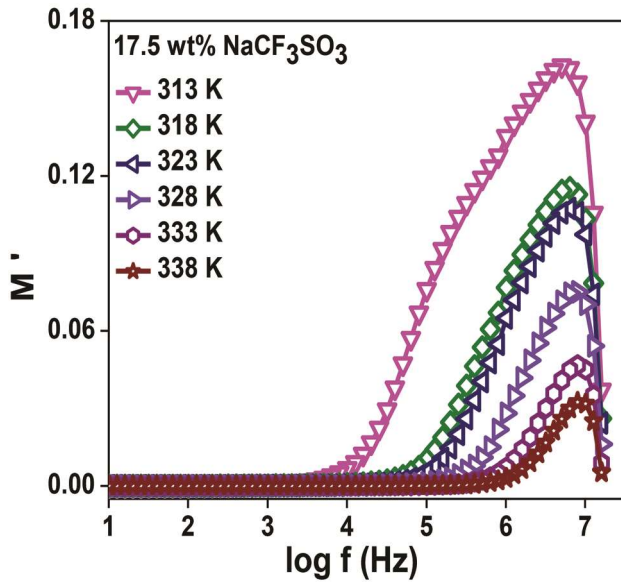


Fig. 14 – Frequency versus M' plots for sample with 17.5 wt% salt concentration at different temperature.

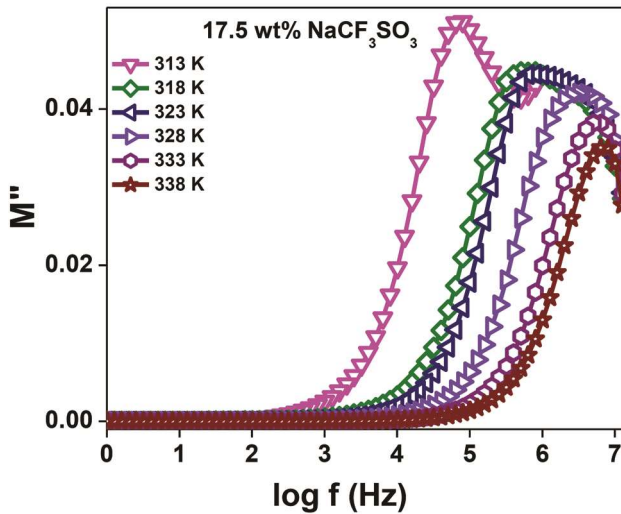


Fig. 15 – Frequency versus M'' plots for sample with 17.5 salt at different temperatures.

$$\phi(t) = \exp \left[- \left(\frac{t}{\tau_\sigma} \right)^\beta \right]; 0 < \beta < 1 \quad \dots (14)$$

The asymmetric and-out-spread shape of M'' peak can be approximated by stretched exponential Kohlraush-Williams-Watts (KWW) function⁴⁴ where, $\phi_{KWW}(t)$ is the stretched exponential function of the electric field, t is the time and β is Kohlraush-Williams-Watts exponent. The β parameter has been interpreted either as representatives of a distribution of relaxation times or as characteristic of cooperative motions between charge carriers. The relaxation

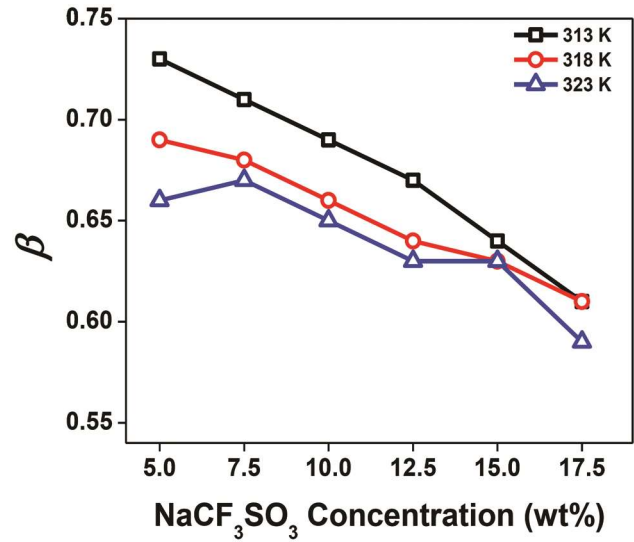


Fig. 16 – KWW parameter (β) versus salt concentration for different temperatures.

parameter, which increases with decrease in width of the relaxation time distribution and its values show the degree of deviation from ideal Debye behavior and $\beta \sim 0$ illustrates maximum interaction between ions and the factors affecting the ion transport²⁹. Calculated values of β for samples with varying salt concentrations at different temperatures are plotted in Fig. 16. β values decrease with increase in salt concentration as well as temperature. β values show a considerable deviation from Debye behavior and are in consonance with the results of Z'' and M'' vs $\log f$ plots.

3.6 Scaling of modulus

Scaling of dielectric relaxation spectra is carried out to present whether the relaxation processes are independent/dependent of charge carrier concentration and/or thermally activated. Scaling provides a view into composition and temperature dependence of ion relaxation dynamics. We have used Ghosh's⁴⁵ scaling approach for scaling imaginary part of the modulus function. The scaling function is defined as:

$$\frac{M'}{M''} = F \left(\frac{f}{f_{max}} \right) \quad \dots (15)$$

modulus M'' on y-axis is scaled by peak maximum value M''_{max} and frequency is on x-axis which is scaled by f_{max} which is the frequency of M''_{max} . Figure 17 shows scaling of M'' as a function of salt concentration. The M'' plots do not merge onto a master plot but exhibit slightly different relaxation

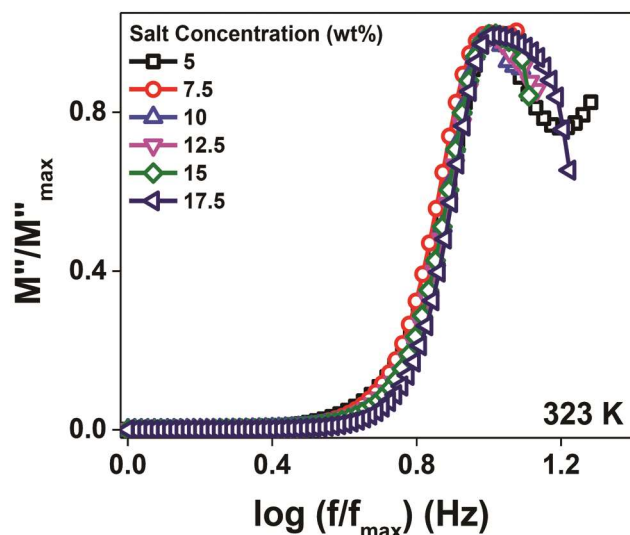


Fig. 17 – Scaling of M'' plots as function of temperature.

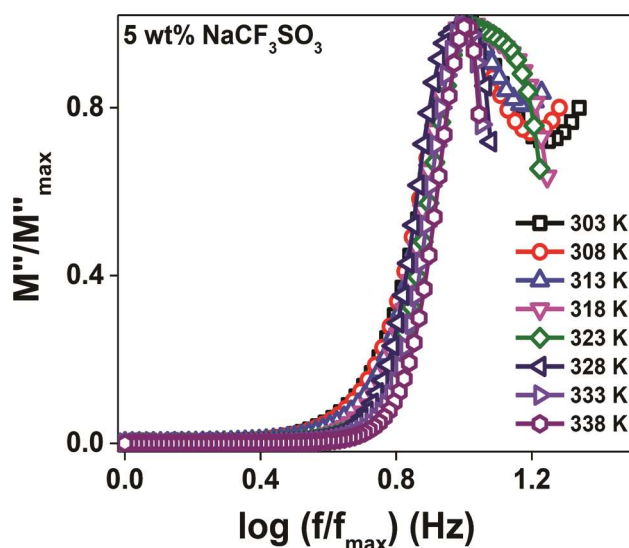


Fig. 18 – Scaling of M'' plots as function of salt concentration.

behaviour for different salt concentrations. Normalized plots do not form a perfect master curve which indicates that the relaxation process is dependent on salt concentration in the present electrolytes. Figure 18 shows scaling of M'' for sample with 17.5 wt% NaCF_3SO_3 at different temperatures. The scaled plots M'' plots fail to fall into single master curve which indicates that the relaxation process are temperature dependent.

4 Conclusions

Dielectric relaxation and modulus studies of PEO-PAM based sodium salt electrolyte films prepared by solution cast technique were studied.

Measured under identical experimental conditions, the films of $[\text{PEO}:\text{PAM}]\text{-NaCF}_3\text{SO}_3$ exhibit an enhanced dielectric response as compared to pure PEO:PAM. Dielectric loss increases with temperature. Stretched exponential decay and peaks in M'' spectra attribute the strong coupling between ionic and polymer segmental motions in the present ionic conductors. The value of dielectric constant increases with the increase in NaCF_3SO_3 salt in the electrolyte films and high conductivity indicates the usefulness of these films as a material for probable Na-solid polymer electrolytes. Relaxation process in PEO:PAM- NaCF_3SO_3 electrolyte films is temperature as well as concentration dependent.

References

- 1 Wright P, *Electrochim Acta*, 43 (1998) 1137.
- 2 Kiran KK, Ravi M, Pavani Y, Bhavani S, Sharma AK & Rao V V R N, *Physica B*, 406 (2011) 1706.
- 3 Osman Z, Anzor N M, Chew K W & Kamarulzaman N, *Ionics*, 11(2005) 431.
- 4 Sivakumar M, Subadevi R, Rajendran S, Wu H C & Wu N L, *Europ Polym J*, 43 (2007) 4466.
- 5 Ramesh S, Leen K H, Kumatha K & Arof A K, *Spectrochim Acta A*, 66 (2007) 1237.
- 6 Rajendran S, Kannan R & Mahendran O, *Mater Lett*, 49 (2001) 172.
- 7 Radhakrishnan S & Venkatachalapathy P D, *Polymer*, 37 (1996) 3749.
- 8 Sumathi S, Sethuprakash V, Basirun W J, Zainol I & Sookhakistan M, *J Sol-Gel Sci Technol*, 69 (2014) 480.
- 9 Virya A & Lian K, *Electrochem Commun*, 74(2017) 33
- 10 Fergus J W, *Solid State Ionics*, 227 (2012) 96.
- 11 Prasanth R, Shubha N, Hng H H & Srinivasan M, *Europ Polym J*, 49 (2013) 307.
- 12 Kim C S, Yoo J S, Jeong K M, Kim K & Yi C W, *J Power Sources*, 289 (2015) 41.
- 13 Kim S, Hana T, Jeonga J, Lee H, Ryoua M H & Lee Y M, *Electrochim Acta*, 241 (2017) 553.
- 14 Kumar D & Hashmi SA, *Solid State Ionics*, 181 (2010) 416.
- 15 Vignarooban K, Kushagra R, Elango A, Badami P, Mellander B E, Xu X, Tucker T G, Nam C & Kannan A M, *Int J Hydrogen Energy*, 41 (2016) 2829.
- 16 Hashmi S A & Chandra S, *Mater Sci Eng B*, 34 (1995) 18.
- 17 Praveen D, Bhat S V & Ramakrishna D, *Ionics*, 19 (2013) 1375.
- 18 Kiran K K, Ravi M, Pavani Y, Sharma A K & Narasimha R V V R, *J Memb Sci*, 454 (2014) 200.
- 19 Fauteux D, Lupien M D & Robitaille C D, *J Electrochem Soc*, 134 (1987) 2761.
- 20 Marinov Y G, Hadjichristov G B, Petrov A G, Koduru H K, Marino L & Scaramuzza N, *IOP J Phys Conf Ser*, 794 (2017) 2020.
- 21 Véleza J F, Álvarez L V, Río C D, Herradón B, Mann E & Morales E, *Electrochim Acta*, 241 (2017) 517.

- 22 Wang C, Yeh Y, Wongittharom N, Wang Y, Tseng C, Lee S, Chang W S & Chang J K, *J Power Sources*, 274 (2015) 1016.
- 23 Devaux D, Bouchet R, Glé D & Denoyel R, *Solid State Ionics*, 227 (2012) 119.
- 24 Fetters L J, Lohsey D J & Colbyz R H & Mark J E, *Physical properties of polymers handbook*, 2ndEdn, (Springer: New York), (2007) 447.
- 25 Cullity B D & Stock S R, *Elements of X-ray diffraction*, 3rdEdn, (Prentice Hall: New Jersey) (2001) 99.
- 26 Raghu S, Subramanya K, Ganesh S, Nagaraja G K & Devendrappa H, *Radiat Phys Chem*, 98 (2014) 124.
- 27 Alexander L E, *X-ray Diffraction methods in polymer science*, (John Wiley: New York) (1969) 379.
- 28 Kumar A, Saikia D, Singh F & Avasthi D K, *Solid State Ionics*, 177 (2006) 2575.
- 29 Sharma P, *Study of conduction mechanism in PEO-PMMA polymer blend nano-composite electrolytes*, Ph D Thesis, The Maharaja Sayajirao University of Baroda, 2013.
- 30 Pradeepa P, Edwinraj S & Ramesh P M, *Chin Chem Lett*, 26 (2015) 1191.
- 31 Jonscher A K, *Nature*, 267 (1977) 673.
- 32 Pant M, Kanchan D K & Gondaliya N, *Mater Chem Phys*, 115 (2009) 98.
- 33 Sharma P, Kanchan D K & Gondaliya N, *Ionics*, 19 (2013) 777.
- 34 Navaratnam S, Ramesh K, Ramesh S, Sanusi A, Basirun W J & Arof A K, *Electrochim Acta*, 175 (2015) 68.
- 35 El-Nahass M M, El-Deeb A F, El-Sayed H E A & Hassanien A M, *Physica B: Condens Matter*, 388 (2007) 26.
- 36 Coelho R, *Revue Phys Appl*, 18 (1983) 137.
- 37 Stevels J M & S Flugge, *Handbuch der physik*, Edn, (Springer: Berlin), (1957) 350.
- 38 Molak A, Paluch M, Pawlus S, Klimonko J, Ujma Z & Gruszka I, *J Appl Phys*, 38 (2005) 1450.
- 39 Macedo P B, Moynihan C T & Bose R, *Phys Chem Glasses*, 13 (1972) 171.
- 40 Mc Crum N G, Read B E & Williams G, *Anelastic and dielectric effects in polymeric solids*, (Dover: New York) 1991.
- 41 Hodge I M, Ngai K L & Moynihan C T, *J Non-Cryst Solids*, 351 (2005) 104.
- 42 Tapabrata D, Satya T, Marian P, Sidhartha S J & Dillip K P, *Electrochim Acta*, 202 (2016) 147.
- 43 Das S & Ghosh A, *Electrochim Acta*, 171 (2015) 59.
- 44 Gondaliya N, Kanchan D K, Sharma P & Joge P, *J Appl Polym Sci*, 125 (12) 1513.
- 45 Karmakar A & Ghosh A, *Curr Appl Phys*, 12 (2012) 539.

Conductivity enhancement in Na⁺-blend electrolyte system via addition of (EC+PC) plasticizers

Cite as: AIP Conference Proceedings **2115**, 030234 (2019); <https://doi.org/10.1063/1.5113073>

Published Online: 12 July 2019

Gargi Dave, C. Maheshwaran, and Dinesh Kanchan



View Online



Export Citation

ARTICLES YOU MAY BE INTERESTED IN

[Green display device technology in Er³⁺ doped TPTiO glass under 808 nm laser excitation](#)

AIP Conference Proceedings **2115**, 030232 (2019); <https://doi.org/10.1063/1.5113071>

[Bismuth modified physical and optical properties of barium boro-tellurite glasses](#)

AIP Conference Proceedings **2115**, 030255 (2019); <https://doi.org/10.1063/1.5113094>

[Influence of LiCl on electrical properties of dysprosium doped calcium bismo borate glasses](#)

AIP Conference Proceedings **2115**, 030241 (2019); <https://doi.org/10.1063/1.5113080>

AIP | Conference Proceedings

Get **30% off** all
print proceedings!

Enter Promotion Code **PDF30** at checkout



Conductivity Enhancement In Na⁺-Blend Electrolyte System Via Addition Of (EC+PC) Plasticizers

Gargi Dave, C Maheshwaran and Dinesh Kanchan^{a)}

Solid State Ionics & Glass Research Laboratory, Physics Department, Faculty of Science, The M. S. University of Baroda, Vadodara - 390002, India.

^{a)}Corresponding author: dkkanchan.ssi@gmail.com

Abstract. Effect of EC-PC plasticizers on electrochemical properties of sodium triflate (NaCF₃SO₃), based PEO-PAM blend electrolyte system has been investigated. Polymer electrolyte samples [PEO₅₀ + PAM₅₀ + 12.5 wt% NaCF₃SO₃ + x wt% (1:1/EC: PC)] plasticizers with x varying as 5, 10, 15, 20, 25 according to wt% have been prepared using solution cast technique. Differential Scanning Calorimetry has been used to characterize the samples. The electrical properties of materials are studied using impedance spectroscopy in the frequency range of 20 Hz to 2 MHz from room temperature to 333 K. The conductivity increases with the addition of plasticizer in the electrolyte films. Maximum ambient temperature conductivity of 5.74×10⁻⁴ S/cm is observed in sample with 15 wt% plasticizer.

INTRODUCTION

Solid Polymer Electrolytes (SPEs) have been most widely investigated class of polymer electrolytes for a very long time. Researchers are constantly working on achieving enhanced conductivity values in traditional PEO based SPE for their application as electrolyte material in commercial electrochemical devices. Basic drawback of such PEO based systems is poor ambient temperature conductivity due to its semi-crystalline nature. Efforts made to increase the amorphous phase of PEO and to decrease the crystallinity by blending of PEO with an amorphous polymer, addition of plasticizers, irradiating the electrolyte system, co-polymerization etc. Blending of PEO with an amorphous polymer like PAM results in an overall increase in the conductivity via suppression of crystallinity [1]. Further the electrochemical properties of such a blend electrolyte system can be enhanced by addition of low molecular weight, high dielectric constant diluents [2-5]. These solvents, popularly known as plasticizers, are organic chemicals which remain in liquid phase inside the host matrix and pave conduction pathways for the mobile ion species. Low molecular weights of the plasticizer make sure that they are embedded completely with the system and their high dielectric constant increases charge storage capacity of the electrolyte. Plasticizers also should have low viscosity so that, the polymer chains can flex readily and produce a greater free volume for ion motion. Reports on various plasticizers have shown that incorporation of ethylene carbonate (EC) and propylene carbonate (PC) are premiere technology to achieve enhanced electrochemical properties of the system [2]. PC has higher dielectric constant than that of EC and EC is less viscous as compared to PC. Favourable properties of both liquids compliment each-other well and hence in the present work, we investigate combined effect of EC+PC plasticizers on conductivity of [(PEO₅₀: PAM₅₀) + (NaCF₃SO₃)_{12.5}] blend electrolyte system.

EXPERIMENTAL DETAILS

Polyacryl amide (PAM; Molecular Weight =50,00,000 gmol⁻¹) from Hi-Media, Polyethylene Oxide (PEO; Molecular Weight = 300,000 gmol⁻¹) from Alfa Aesar, Sodium trifluoromethanesulfonate (NaCF₃SO₃), Ethylene Carbonate (EC; Molecular Weight =88.06 gmol⁻¹) and Propylene Carbonate (PC; Molecular Weight =102.9 gmol⁻¹) from Sigma Aldrich are obtained. All chemicals are used as received. Polymers and the salt as a whole are dissolved

in deionized water and stirred for 24h continuously to achieve a homogeneous mixture. Solutions thus prepared with different amounts of plasticizer (1:1/ (w/w) (EC+PC)) are solution casted into Teflon petri dish. Free standing films of 160-220 μm thickness have been obtained after evaporating all traces of solvent at room temperature. The obtained films were stored in desiccator under vacuum for later use for measurement. SEM images are recorded on Hitachi SU 1510 instrument at a magnification of 2000X at 10 kV after gold coating on to the films. Agilent E4980A Precision LCR meter instrument has been used for impedance measurement in the frequency range of 20 Hz to 2 MHz from ambient temperature up to 333 K. For this, the sample is placed under spring pressure between two blocking silver electrodes (dia = 1.2 cm).

RESULTS AND DISCUSSION

Differential Scanning Calorimetry (DSC)

DSC thermograms have been used to study melting temperatures of the blend electrolyte system. All the samples have two endothermic peaks, one in the temperature range 48.8 $^{\circ}\text{C}$ to 55.6 $^{\circ}\text{C}$ corresponding to the melting temperature of PEO and the other peak in the temperature range 231.6 $^{\circ}\text{C}$ to 242.3 $^{\circ}\text{C}$ corresponding to the PAM melting temperature. Change in crystallinity with addition of plasticizer in polymer electrolyte systems is a largely discussed behaviour [3], hence the values of degree of crystallinity are reported in Table 1. The values of degree of crystallinity and melting temperature are decreasing and clearly suggest a good miscibility of both polymers and intercalation of plasticizer in the blend electrolyte system.

TABLE 1. Values of melting point and degree of crystallinity of un-plasticized and plasticized electrolytes

Concentration of (EC+PC) in wt%	Value of melting temperature T_m ($^{\circ}\text{C}$)		Degree of crystallinity χ_c (PEO)	Degree of crystallinity χ_c (PAM)
	Corresponding to PEO	Corresponding to PAM		
Un-plasticized	55.6	232.6	51.2	48.8
5	53.2	238.2	46.5	49.1
10	51.2	232.1	38.4	46.3
15	48.8	231.6	33.2	41.8
20	53.6	236.9	40.1	44.2
25	54.4	242.3	42.7	41.1

SEM

Figures. 1(a) and (b) show the SEM micrographs of blend polymer electrolyte (BPE) samples with 10wt% and 15 wt% EC+PC respectively. The micrographs depict a clear change in morphological structure of the polymer films with addition of plasticizer. More number of elongated structure and voids are observed for sample with 15 wt% (EC+PC) than that for 10wt%, which depicts higher amorphous nature of the sample. It is revealed that as we increase the (EC+PC) amount, the amorphicity increases and reaches to maximum at 15 wt% as also shown in Fig. 1(b). The amorphicity of the films decreases beyond 15 wt%.

Conductivity

Impedance has been measured at different temperatures in the frequency range of 20 Hz to 2 MHz. Fig. 2 shows conductivity as a function of plasticizer content. Conductivity of BPE increases with increasing amount of EC+PC upto 15 wt% and decreases for higher wt% (EC+PC) content. Highest conductivity value of 5.74×10^{-4} S/cm is noted for sample with 15 wt% plasticizer at 333K temperature. Initial increase in conductivity with increase in plasticizer content can be attributed to enhanced diffusivity of the Na^+ -ions through plasticizer rich region. Liquid phase of the plasticizer makes it easy for the mobile ions to hop through the vacant sites and thus contribute to increase in conductivity of the BPEs. Above 15 wt% (EC+PC), a decrease in ionic conductivity is observed. The reason of this drop is the increased interaction between mobile ions and the plasticizer and a decreased interaction between salt and polymer. This gives the polymer chains a chance to reorient themselves in an orderly manner and this restores crystallinity of the system [4].

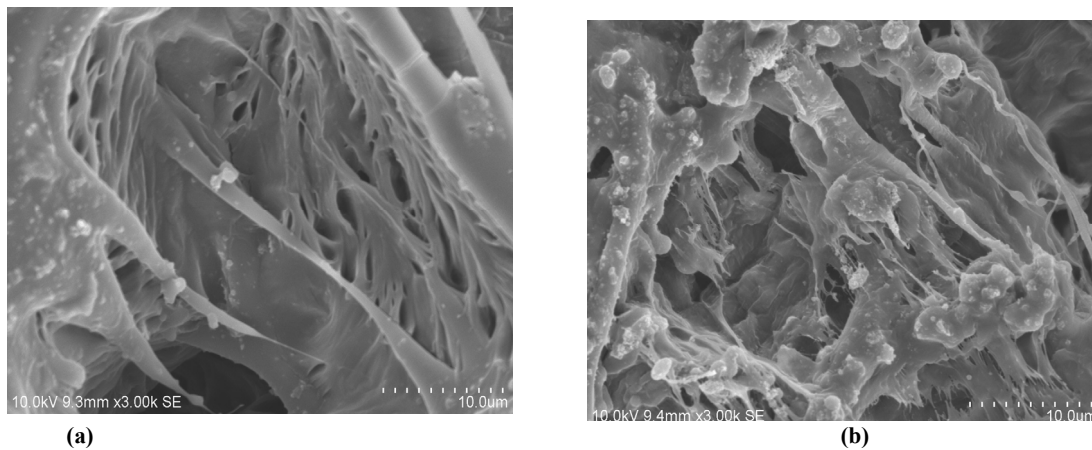


FIGURE 1. (a) SEM Micrograph of sample with 10 wt% (EC+PC) content (b) SEM Micrograph of sample with 15 wt% (EC+PC) content

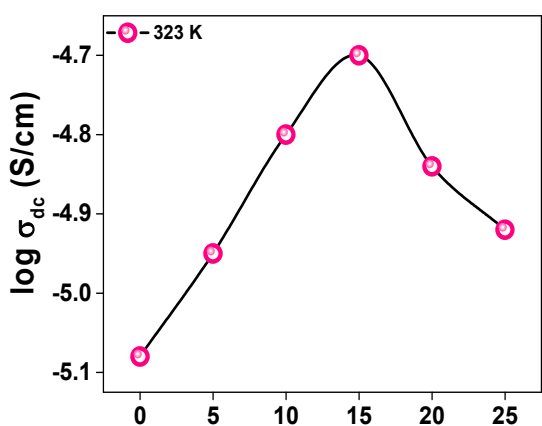


FIGURE 2. Conductivity as a function of (EC+PC) content

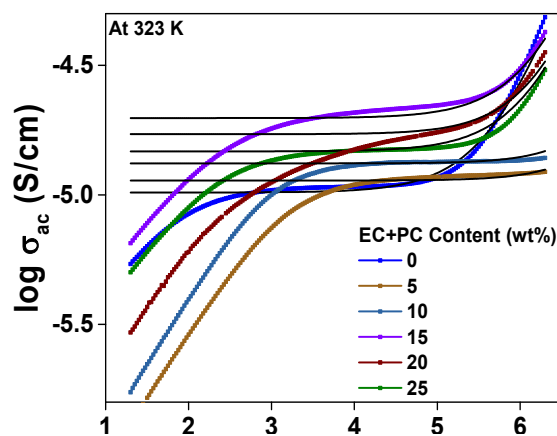


FIGURE 3. AC Conductivity plots of un-plasticized and plasticized BPE samples

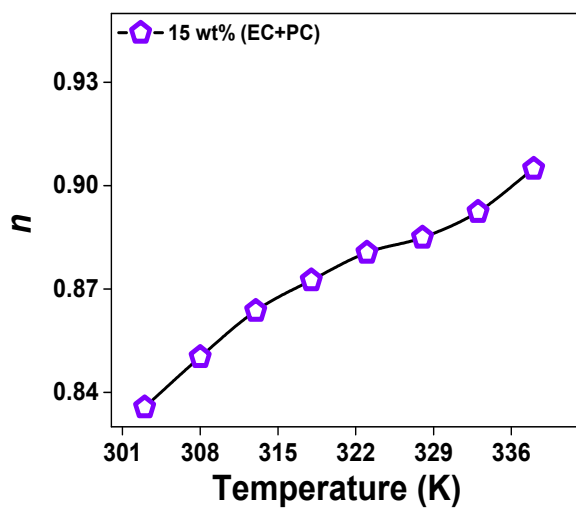


FIGURE 4. Power law exponent as a function of temperature

Frequency dependent ac conductivity of the system un-plasticized and plasticized at different concentrations of (EC+PC) is shown in Fig.3. Two different regions (region 1-2) are observed in all the samples. Low frequency region is observed due to the electrode-electrolyte interface. Higher frequency region depicts the dispersive nature of the system. At higher frequencies, probability of successful ion jump decreases and the conductivity shows dispersive behavior with frequency. Mobility of the charge carriers is high near the relaxation times at higher frequencies and so the conductivity increases with increase in frequency. Variation of conductivity with frequency can be well interpreted from Jonscher's Universal Power Law [5].

$$\sigma(\omega) = \sigma_0 + A\omega^n \quad (1)$$

where $\sigma(\omega)$ is the value of AC conductivity, σ_0 depicts DC conductivity, A is a constant for particular temperature and n is the power law exponent related to degree of interaction amongst mobile ions and lattice around them [5, 6]. The values of power law exponent n as a function of temperature for sample with 15 wt% (EC+PC) are shown in Fig.4. Since the calculated values of exponent n lie in the range .6 to .9, the correlation motion is sub diffusive and indicates a preference on the part of the ions that has hopped away to return to where it started. Non Overlapping Small Polaron Tunneling (NSPT) model [7] describes the conduction process in the present system where, the value of power law exponent n increases with increase in temperature.

CONCLUSION

(EC+PC) plasticized PEO-PAM- NaCF₃SO₃ system shows good intercalation of plasticizers in blend electrolyte system. The increasing (EC+PC) amount in the films decreases their crystallinity and an increase in conductivity is observed with increase in plasticizer content. Conductivity value reaches an optimum at 15 wt% (EC+PC) content and shows a decrease thereafter. The process of conduction follows the Non Overlapping Small Polaron Tunneling (NSPT) model. The electrolyte system may be a good candidate for sodium batteries.

REFERENCES

1. G. G. Kumar, N. Munichandraiah, *Journal of Electroanalytical Chemistry* **495**, 42-50 (2000).
2. X. Wang, Y. Zhang, Q. Xu, J. Xu, B. Wu, M. Gong, J. Chu, S. Xiong, *Journal of Photochemistry and Photobiology A: Chemistry* **311**, 112-117 (2015).
3. D. K. Pradhan, R. N. P. Choudhary, B. K. Samantaray, N. K. Karan, R. S. Katiya, *International Journal of Electrochemical Science* **2**, 861-871 (2007).
4. R. Muchakayala, S. Song, S. Gao, X. Wang, Y. Fan, *Polymer Testing* **58**, 116-125 (2017).
5. K. Jonscher, *Nature* **267**, 673-679 (1977).
6. M. Pant, D. K. Kanchan, N. Gondaliya, *Materials Chemistry and Physics* **115**, 98-104 (2009).
7. S. Murugavel, M. Upadhyay, *Journal of the Indian Institute of Science* **91**, 303-317 (2011).

Conductivity studies of blend polymer electrolyte system irradiated with swift heavy O^{6+} ion beam

Gargi Dave, D. K. Kanchan, and F. Singh

Citation: [AIP Conference Proceedings](#) **1942**, 140087 (2018); doi: 10.1063/1.5029218

View online: <https://doi.org/10.1063/1.5029218>

View Table of Contents: <http://aip.scitation.org/toc/apc/1942/1>

Published by the [American Institute of Physics](#)

Conductivity Studies of Blend Polymer Electrolyte System Irradiated with Swift Heavy O⁶⁺ ion beam

Gargi Dave^{1a}, D.K. Kanchan¹ and F. Singh²

¹ *Solid State Ionics & Glass Research Laboratory, Physics Department, Faculty of Science, The M. S. University of Baroda, Vadodara - 390002, India*
² *Inter University Accelerator Center, Aruna Asaf Ali Marg, New Delhi-110067, India*

^aCorresponding author: dkkanchan.ssi@gmail.com

Abstract. Effect of swift heavy ion irradiation on conductivity of blend electrolyte system [(PEO₅₀:PAM₅₀) +x%(NaCF₃SO₃), x=5, 7.5, 10, 12.5, 15, 17.5] with O⁶⁺ ion at four different fluences is investigated. The samples are prepared using solution cast technique and films are subjected to irradiation at room temperature. Conductivity is measured for pristine and irradiated sample as a function of frequency in the range 2 Hz – 2MHz from ambient temperature up to 338 K. It is observed that conductivity increases with fluence. Highest conductivity value is found to be 3.2375×10⁻⁴ S/cm at 338 K for fluence of 1× 10¹² ions/cm² for sample containing 17.5 wt% NaCF₃SO₃. SEM and X-ray diffraction techniques have been conducted for the blend electrolytes before and after irradiation to completely understand the changes in the surface morphology.

INTRODUCTION

Since Fenton [1] suggested fast ion conduction in PEO based electrolytes, it has been investigated as one of the most suitable matrix for electrolyte systems. But poor room temperature conductivity of PEO limits its application as an electrolyte. Polymer blending, plasticization, dispersion with nano particles and irradiation by high energy particles are the different techniques for decreasing the crystallinity and show superior properties as compared to the parent polymers. The amorphous region of the polymers is enhanced by polymer blending which results in overall good conductivity of the electrolyte system [2]. In the present study, we report the effect of irradiation with swift heavy O⁶⁺ on structural properties and conductivity of PEO-PAM blend electrolyte system containing sodium triflate as salt without any plasticizer in it.

EXPERIMENTAL DETAILS

Polyacryl amide (PAM; 50,00,000) from HiMedia, Polyethylene Oxide (PEO; 300,000) from Alfa Aesar and Sodium trifluoromethanesulfonate (NaCF₃SO₃) from Sigma Aldrich are obtained. All chemicals are used as received. The solid NaCF₃SO₃ doped blend polymer electrolyte (BPE) have been prepared by solution cast technique using distilled water as solvent. Free standing films of 160 μm thickness have been obtained after evaporating all traces of solvent. SEM images are recorded on Hitachi SU 1510 instrument at a magnification of 2000X at 10 kV after gold coating on to the films. Agilent E4980A Precision LCR meter instrument has been used for impedance measurement in the frequency range of 20 Hz - 2 MHz from ambient temperature to 323 K. For this, the sample is placed under spring pressure between two blocking silver electrodes (dia = 1.2 cm). Bulk electrolyte resistance and low frequency linear response are obtained from Nyquist plots by fitting to appropriate equivalent circuit.

For ion beam irradiation, free standing films are cut into 1 cm × 1 cm segments and mounted on the ladder maintaining a distance of 1 cm between all the samples. Irradiation with 80 MeV swift heavy O⁶⁺ ion beam is carried out using material science beam line facility of pelletron accelerator at IUAC, New Delhi. Irradiation has been carried out at four different fluences, namely 1× 10¹¹, 3× 10¹¹, 1× 10¹², 2× 10¹² ions/cm².

RESULTS AND DISCUSSIONS:

XRD Studies

Fig. 1 shows X-ray diffractograms of pristine and irradiated blend electrolyte samples with 10 wt% salt concentration. Two prominent peaks are observed in all the electrolyte films. It is observed that the intensity of the peak at $2\theta \approx 23^\circ$ does not vary significantly after irradiation. The intensity of peak at $2\theta \approx 31^\circ$ decreases upto fluence of 3×10^{11} ions/cm² and decreases at fluence beyond it. It is observed that the value of intensity of the peaks and the average crystallite size are decreasing continuously with fluence which is an indication of increase in amorphosity of the system. Average crystallite size (L) is calculated using the Scherrer formula [3, 4].

$$L = \frac{k\lambda}{\beta \cos \theta} \quad (1)$$

where, β is the FWHM of the peak (in radian) and k is the shape factor whose value is assumed to be 0.9 for calculating the parameters. The average inter-chain separation is calculated using the following equation [5].

$$R = \frac{5\lambda}{8 \sin \theta} \quad (2)$$

Values of average crystallite size, d-spacing and average inter-chain separation are presented in table.1

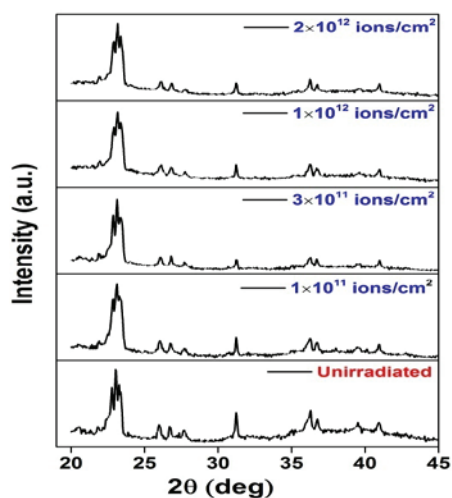


FIGURE 1. XRD diffractograms of pristine and irradiated samples

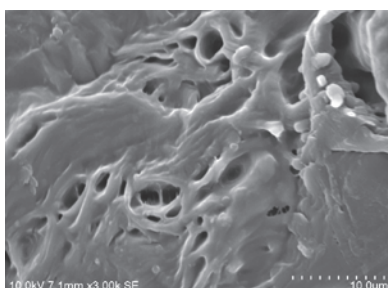


FIGURE 2. . SEM Micrograph of sample with 17.5wt% salt in pristine form

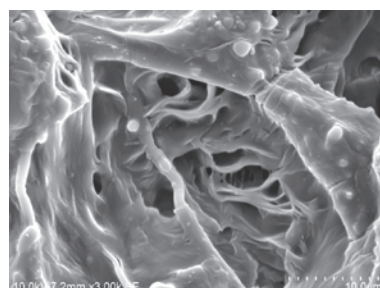


FIGURE 3. SEM Micrograph of sample with 17.5wt% salt concentration at fluence of 1×10^{12} ions/cm²

TABLE 1. XRD parameters of pristine and irradiated samples and Activation Energy

Sample	2θ	d (Å)	L (nm)	R (Å)	Activation Energy (eV)
Pristine	30.141	4.015	31.034	5.266	1.85
1×10^{11} ions/cm ²	30.514	4.020	24.933	5.260	1.85
3×10^{11} ions/cm ²	30.723	4.290	22.929	5.256	1.80
1×10^{12} ions/cm ²	30.996	4.308	20.704	5.261	1.75
2×10^{12} ions/cm ²	31.012	4.336	19.012	5.254	1.79

SEM studies

Electron Microscopy has been found to be useful in understanding the morphological changes in the polymer electrolytes upon Swift Heavy Ion (SHI) irradiation. The SEM exhibits changes in the grain size, surface morphology, agglomeration, displacement of polymer molecules and the formation of porous structures. The microstructure also shows highly entangled and disordered small pore size before irradiation of electrolyte films and elongated granular microstructure with larger pore size after irradiation. Figs. 2 and 3 show the SEM micrographs of sample with 17.5 wt% salt in pristine form and irradiated samples at a fluence of 1×10^{12} ions/cm². The micrographs depict a clear change in morphological structure of the polymer films with irradiation. Elongated structure and voids are formed after irradiation. The increased porosity upon ion irradiation indicates the formation of more polymer electrolyte interface area in the same volume and provides the better connectivity of the electrolyte through the polymer providing higher conductivity.

Conductivity

Frequency dependent AC conductivity of the sample with 17.5 wt% salt at various fluences is shown in Fig. 4(a). Two different regions (Region 1-2) are observed in all the samples. Low frequency region is observed due to the electrode-electrolyte interface. Higher frequency region depicts the dispersive nature of the system. After irradiation by SHI, the energy deposited in the polymer causes chain scissioning and produces radicals. At low fluence, chain scissioning predominates because of wide separation of chains. However, with the increase of the fluence, radical concentration increases resulting in formation of closely spaced radicals along ion-track which eventually make the adjacent polymer chains to cross-link. Increase in ionic conductivity at lower fluences can be ascribed to the fact that SHI irradiation breaks large polymer chains to smaller size due to chain scissioning effect [6]. This induces the larger segmental motion of the polymer back-bone resulting in the increase in ionic conductivity. However at fluence of 2×10^{12} ions/cm², cross-linking of the polymer chain dominates which results in reduction in ionic conductivity. Variation in AC conductivity for various salt concentrations for fluence of 1×10^{12} ions/cm² is shown in Fig. 4(b). The conductivity of the pristine sample of 17.5% salt is 2.68×10^{-5} S/cm which increase to 2.34×10^{-4} S/cm when subjected to fluence of 1×10^{12} ions/cm². An increase of 1 order has been observed in conductivity values for all samples.

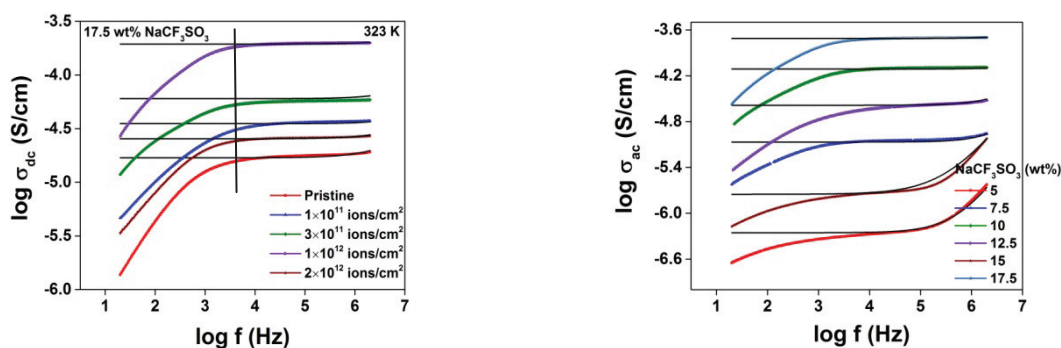


FIGURE 4(a). AC Conductivity for sample with 17.5 wt% salt at different fluences **(b)** AC Conductivity at various salt concentration for fluence of 1×10^{12} ions/cm²

Temperature dependence of conductivity for 17.5 wt% at different fluences is plotted in Fig.5 (a). The plot of $\log \sigma$ vs. $1000/T$ is evidently not a straight line according to Arrhenius relation. The typical curvature behavior of the plots can be explained by VTF relation which indicates that the ion conduction strongly depends on polymer segmental motion [7]. Increase in temperature leads to faster polymer chain relaxation which produces segmental motion [8], leading to an increase in the free volume of the system. Increase in free volume, favours ion movement which results in increase in conductivity with temperature [9]. The VTF relation is given as follows.

$$\sigma = \frac{AT^{1/2}B}{k(T - T_0)} \quad (3)$$

where A is pre-exponential factor, B is the apparent activation energy associated with the hybrid energy, k is the Boltzmann constant, T_0 is the ideal glass transition temperature, typically taken to be 50 K below T_g . Fig.5 (b) shows conductivity and activation energy behaviour with fluence. Conductivity increases with increase in fluence upto 1×10^{12} ions/cm² and then decreases for further fluence. Activation energy values for 17.5 wt% salt sample at various fluences are given in Table1.

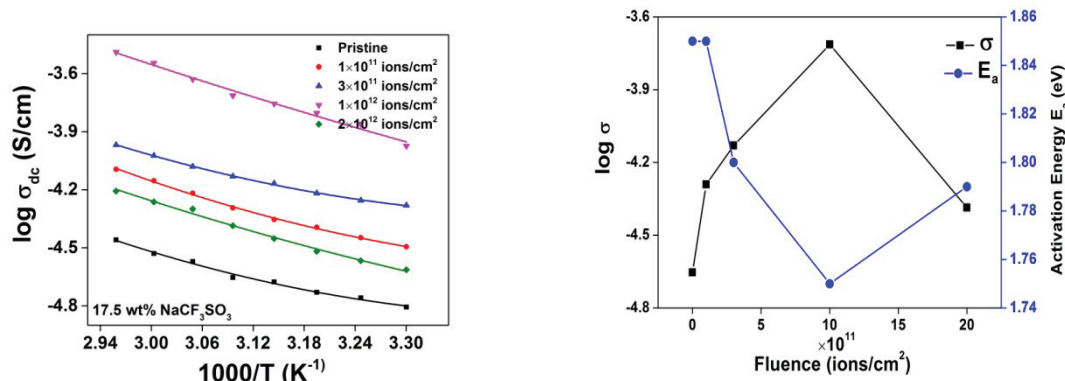


FIGURE 5(a). DC Conductivity for sample with 17.5 wt% salt at different fluences (b) Conductivity and Activation energy as a function of fluence

CONCLUSIONS

Conductivity of blend electrolyte system [(PEO: PAM) +NaCF₃SO₃] with SHI O⁶⁺ ion at four different fluences is investigated. XRD analysis depicts that with the increase of fluence, the average crystallite size decreases. SEM micrographs show the increased porosity upon ion irradiation indicating the formation of more polymer electrolyte interface area in the same volume. The increase in ionic conductivity at lower fluencies is due to the larger segmental motion of the polymer back-bone and at fluence of 2×10^{12} ions/cm², cross-linking of the polymer chain dominates which results in reduction in ionic conductivity.

ACKNOWLEDGMENTS

This work has been carried out under Project BTR NO. 54319 supported by UGC, New Delhi. Authors extend their sincere gratitude to IUAC, New Delhi for providing Ion-beam facilities.

REFERENCES

1. D. E. Fenton , M. Parker , P. V. Wright, *Polymer* **14**, 589-592 (1973)
2. K. K. Kiran, M. Ravi, Y. Pavani, S. Bhavani, A. K. Sharma, V. V. R. N. Rao, *Physica B* **406** pp. 1706 (2011)
3. B. D. Cullity, S. R. Stock, in *Elements of X-ray Diffraction, Third Edition*, (Addison-Wesley Publishing Company Inc, Boston, 2001), pp. 99
4. S. Raghu, K. Subramanya, S. Ganesh, G. K. Nagaraja, H. Devendrappa, *Radiation Physics and Chemistry* **98** pp. 124 (2014)
5. L. E. Alexander, in *X-ray Diffraction Methods in Polymer Science*, (John Wiley, NewYork, 1969), pp. 379
6. M. Gaffar, *Nuclear Instruments and Methods in Physics Research Section B: Beam Interactions with Materials and Atoms*, **174**, 507-511 (2001)
7. D. P. Nava, G. Guzmán, J. A. Vazquez, J. Cardoso, B. Gomez, I. Gonzalez, *Solid State Ionics* **90** pp.98 (2016)
8. ASK. Ahmad, A. K. Arof, *Ionic* **16** pp.123(2010)
9. N.H. Idris, H. B. Senin, A. K. Arof, *Ionic* **13** pp. 213 (2007)

Characterization of plasticized PEO-PAM blend polymer electrolyte system

Gargi Dave and Dinesh Kanchan

Citation: [AIP Conference Proceedings](#) **1832**, 140042 (2017); doi: 10.1063/1.4980824

View online: <http://dx.doi.org/10.1063/1.4980824>

View Table of Contents: <http://aip.scitation.org/toc/apc/1832/1>

Published by the [American Institute of Physics](#)

Characterization of Plasticized PEO-PAM Blend Polymer Electrolyte System

Gargi Dave and *Dinesh Kanchan

Department of Physics, Faculty of Science, The M. S. University of Baroda, Vadodara-390002, Gujarat, India
[*dkkanchan.ssi@gmail.com](mailto:dkkanchan.ssi@gmail.com)

Abstract. Present study reports characterization studies of NaCF₃SO₃ based PEO-PAM Blend Polymer Electrolyte (BPE) system with varying amount of EC+PC as plasticizer prepared by solution cast technique. Structural analysis and surface topography have been performed using FTIR and SEM studies. To understand, thermal properties, DSC studies have been undertaken in the present paper

Keywords: Blend Polymer Electrolytes, Sodium Triflate, Thermal properties.

PACS: 72.80.-r, 73.61.-r, 82.35.-x

INTRODUCTION

Recent years have witnessed rising interest in Blend Polymer Electrolyte (BPE) system instead of conventional single polymer based electrolyte. It has been reported that polymer electrolytes prepared using polymer blends exhibited higher conductivity and better mechanical strength compared to electrolytes based on pure polymer [1]. Present system is based on polymers Polyacryl amide (PAM) and Polyethylene Oxide (PEO). PEO is most studied host due to its good ionic conductivity when added by a suitable salt [2]. Polyacrylamide gels are widely used in large number of applications both academic and technological [3]. Blends of these two polymers (PEO/PAM) have not been investigated so far hence, the present system is prepared based on these two polymers PEO and PAM, in which sodium triflate (NaCF₃SO₃) is incorporated as salt plasticized with Ethylene Carbonate and Propylene Carbonate (EC and PC).

EXPERIMENTAL DETAILS

The samples are prepared by taking 50:50 weight percentage concentration of PEO and PAM with 12.5 wt% NaCF₃SO₃ fixed and different amount of plasticizer (EC+PC) taken in 1:1 ratio by solution cast technique. Characterizations have been carried out by using Fourier Transform Infrared (FTIR) spectroscopy and Differential Scanning Calorimetry DSC. SEM micrographs are taken on XL 30 ESEM system.

RESULTS AND DISCUSSIONS

DSC Thermograms of plasticized blend samples are shown in Figure 1. Single endothermic peak of melting temperature (T_m) is observed in all the blend systems. The melting peak of BPE samples is found to shift towards the lower temperature side, which indicates complexation of both polymers in the blend system and decrease in degree of crystallinity too. Degree of crystallinity χ_c is given by;

$$\frac{\Delta H_m}{\Delta H_m^0} = \chi_c$$

where, ΔH_m is the heat of fusion of pristine and plasticized blend samples and ΔH_m^0 is the equilibrium heat of fusion of PEO having value 203 J/g [4]. Table 2 shows values of degree of crystallinity for plasticized blend samples. Decrease in degree of crystallinity, is analogous to increase in amorphousity, in the present system values of degree of crystallinity decrease from 42.86 to 38.26. Figure 2 shows FTIR Spectra of pure PAM and PEO. Peak values for pure polymers are given in Table 1. PAM has two peaks at 1107 cm⁻¹ and 1447 cm⁻¹ corresponding to C-O-C and C-N stretching respectively. A broad peak at 2938 cm⁻¹ is attributed to C-H stretching. A broad band in the region 3014-3600 cm⁻¹ is also observed [5-10]. PEO has peaks at 852 cm⁻¹, 966 cm⁻¹, 1106 cm⁻¹, bands in the region 1220-1360 cm⁻¹, peak at 1454 cm⁻¹, and at 1962 cm⁻¹ corresponding to C-C symmetric stretching, -CH₂ rocking, C-O-C stretching, -CH₂ twisting and wagging, -CH₂ scissoring and asymmetric C-H stretching respectively [5-10]. Figure:3 shows IR spectra of plasticized blend samples and without

plasticization where in, the peaks appear to shift slightly which is an indication of good miscibility of

TABLE 1. Assignments of FT-IR Characterization of Bands of pure PAM and pure PEO.

Wave Number cm-1	Peak Assignment for pure PAM	Wave Number cm-1	Peak Assignment for pure PEO
		852	C-C symmetric stretching
		966	-CH ₂ rocking
1107	C-O-C stretching	1106	C-O-C stretching
1447	C-N stretching	1220-1360	-CH ₂ twisting and wagging
2938	C-H stretching	1454	-CH ₂ scissoring
3014-3600		1962	asymmetric C-H stretching
		2700-2950	C-H asymmetric stretching

both the polymers. Absence of many peaks of pure polymers in the blend system suggests good complexation of salt and plasticizer with polymer blend. With the addition of plasticizer, the intensity of the peaks decrease gradually, this also confirms the increase in amorphous nature of the blend electrolytes with plasticization.

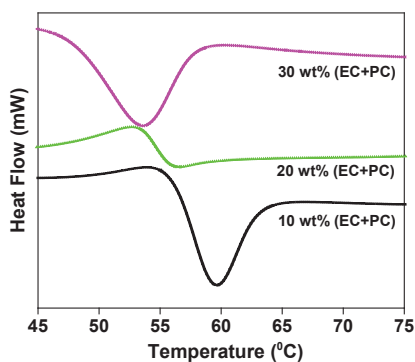


Figure 1. DSC Thermograms of plasticized blend samples.

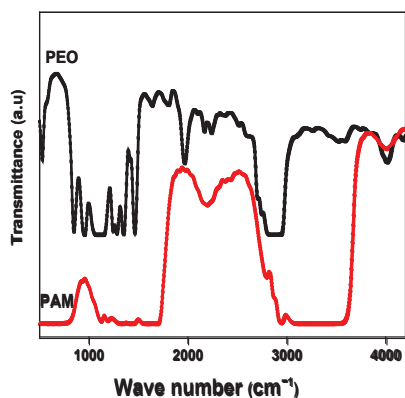


FIGURE 2. IR Spectra of Pure Polymers

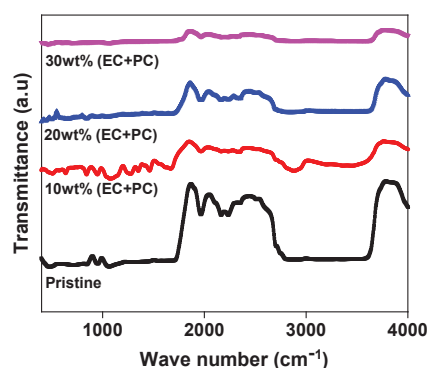


FIGURE 3. IR Spectra of pristine and plasticized blends

SEM micrographs show the electrons interaction with the atoms in the material, producing various signals that can be detected and contain information about the surface topography and composition of the sample. Figure 4 shows SEM image of the 30 wt% plasticized blend sample. Prominent long and sharp features are clearly observed in the sample.

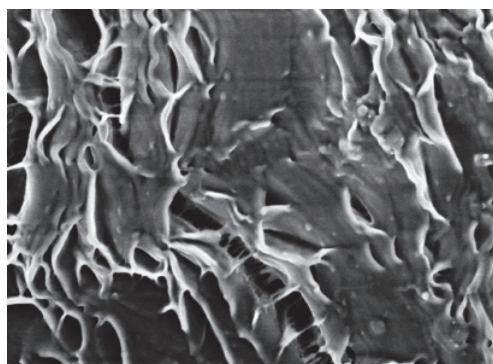


FIGURE 4. SEM micrograph of 30 wt% EC+PC

TABLE 2. Degree Of Crystallinity.

(EC+PC) Concentration In wt%	Degree Of Crystallinity
10	42.87
20	40.16
30	38.26

CONCLUSIONS

NaCF₃SO₃ based PEO-PAM blend electrolyte samples plasticized with EC and PC make a good complexation and show a good miscibility of the constituents. DSC and FTIR results confirm the increase in amorphous nature of electrolyte films. Increase of porous voids in SEM image suggests that the sample may have a good ionic conductivity and can be an useful electrolyte polymer blend system.

ACKNOWLEDGMENTS

The authors are thankful to IUAC, New Delhi, India for their financial support.

REFERENCES

1. S. Rudhziah, N. S. Mohamed and A. Ahmad, *Int.J. Electrochem. Sci* **8**, 421-434 (2013).
2. M. Jaipal Reddy and Peter P. Chu, *Solid State Ionics* **149**, 115-123 (2002).
3. J. Baselga, I. Hernandez-Fuentes, I. F. PiBrola, and M. A. Llorente, *Macromolecules* **20**, 3060-3075 (1987).
4. Y. Song, X. Peng, Y. Lin, B. Wang, and D. Chen, *Solid State Ionics* **76**, 35-39 (1995).
5. Z. Osman, N.M. Ansor, K.W. Chew and N. Kamarulzaman, *Ionics* **11**, 431-435 (2005).
6. Abderlrazek, E.M and Ibrahim H.S, *Physica B* **405**, 4339-4343 (2010).
7. A. V. Parmar, A. Bahadur, K. Kuperkar and P. Bahadur, *European Polymer Journal* **49**, 12-21 (2013).
8. C. Guo, H. Liu, J. Wang and J. Chen, *Journal of Colloid and Interface Science* **209**, 368-373 (1999).
9. M. S. Bostan, E. C. Mutlu, S. H. Kazak, S. S. Keskin, E. T. Oner and M. S. Eroglu, *Carbohydrate Polymers* **102**, 993-1000 (2014).
10. V. M. Mohan, V. Raja, A. K. Sharma and V.V.R.N. Rao, *Ionics* **12**, 219-226 (2006).

Effect of sintering on electrical properties of yttrium doped Li-based NASICON compounds

Dharmesh H. Kothari, , D. K. Kanchan, and , and Gargi Dave

Citation: [AIP Conference Proceedings](#) **1675**, 030059 (2015); doi: 10.1063/1.4929275

View online: <http://dx.doi.org/10.1063/1.4929275>

View Table of Contents: <http://aip.scitation.org/toc/apc/1675/1>

Published by the [American Institute of Physics](#)

A promotional banner for AIP Conference Proceedings. The left side features a background of blue ocean waves with the text 'SUMMER SALE!' in large, bold, blue letters. Below this is the AIP logo (the letters 'AIP' in blue with a vertical bar) followed by 'Conference Proceedings' in a smaller blue font. The right side of the banner is a solid yellow triangle pointing left, containing the text '30% OFF ALL PRINT PROCEEDINGS!' in bold black letters. At the bottom of this yellow section, a white box contains the text 'ENTER COUPON CODE SUMMER2017' in black.

SUMMER SALE!

**30% OFF
ALL PRINT
PROCEEDINGS!**

AIP | Conference Proceedings

ENTER COUPON CODE
SUMMER2017

Effect of sintering on electrical properties of yttrium doped Li-based NASICON compounds

Dharmesh H. Kothari, D.K. Kanchan^{a)} and Gargi Dave

*Solid State Ionics & Glass Research Laboratory, Department of Physics,
Faculty of Science, The M. S. University of Baroda, Vadodara, Gujarat- 390002, India*

^{a)}Corresponding author: dkkanchan.ssi@gmail.com

Abstract. Electrical properties of Lithium based $\text{Li}_{1.3}\text{Al}_{0.3-x}\text{Y}_x\text{Ti}_{1.7}(\text{PO}_4)_3$ (LAYTP) system was prepared using solid state reaction route. The samples were subjected to differing duration of sintering. X-ray diffraction was used to investigate the microstructure while density measurement was performed to determine the effect of sintering on the density of the prepared samples. Electrical properties of the material were studied using impedance spectroscopy, in frequency range 20 MHz to 1 Hz and in temperature range 303 K to 423 K. It was found that sample with least amount of yttrium and which was sintered for least duration had superior conductivity over other samples. It was also found that grain boundary conductivity improved marginally for sample with higher proportion of yttrium heat treated for longer duration.

INTRODUCTION

This NASICON an acronym for (Na like Super Ionic Conductors) is an important class of ceramic material that has been investigated for its role as electrolytes in solid state batteries. It has a rhombohedral structure (space group $R\bar{3}c$) in which Li^+ ions can easily intercalate. These ceramic compounds are structurally robust and can withstand small amount of doping without affecting the overall structure and symmetry. Cation vacancy sites are formed as a result of a structure formed by sharing corner oxygen atoms from two TiO_6 octahedra and six PO_4 tetrahedra. These sites are termed M1 and M2 sites, in general. Lithium based NASICON materials like $\text{LiTi}_2(\text{PO}_4)_3$ (LTP) [1, 2] had been extensively investigated. It was found that doping LTP with trivalent cations like aluminum can increase the Li^+ ionic conductivity [4]. Due to superior Li^+ conductivity ($\sim 10^{-3}\text{S/cm}$), $\text{Li}_{1+x}\text{Al}_x\text{Ti}_{2-x}(\text{PO}_4)_3$ (LATP) system has been extensively investigated for its electrical properties [3, 4]. In earlier studies [5–8] yttrium a trivalent cation (Y^{3+}) was also doped in parent system $\text{Li}_{1.3}\text{Al}_{0.3}\text{Ti}_{1.7}(\text{PO}_4)_3$ (LATP). Y^{3+} tends to replace Al^{3+} cations due to similar valence. In the present study samples of two concentrations (with 1 at% and 15 at% yttrium) are doped in parent system $\text{Li}_{1.3}\text{Al}_{0.3}\text{Ti}_{1.7}(\text{PO}_4)_3$ (LATP) to form $\text{Li}_{1.3}\text{Al}_{0.3-x}\text{Y}_x\text{Ti}_{1.7}(\text{PO}_4)_3$ (LAYTP) system. These samples are subjected to heat treatment (sintering) at 1373 K for durations of 1 hr, 2 hrs and 3 hrs. The effect of these conditions on Li^+ conductivity in grain and grain boundary regions and the density of the material are discussed.

EXPERIMENTAL

Laboratory grade lithium carbonate (Li_2CO_3), ammonium diphosphate ($\text{NH}_4\text{H}_2(\text{PO}_4)$), yttrium oxide (Y_2O_3), titanium oxide (TiO_2), alumina (Al_2O_3) (Loba Chemie, Mumbai, India) were taken according to their weight percentages to create samples of two concentrations (1 at% and 15 at% yttrium) in a cool and dry atmosphere. The weighed powders were mixed and ground using mortar and pestle for 30 min. This mixture was heated in ceramic boats (which exposed the powders to atmosphere) in an electrical furnace upto 873 K for 20 minutes. On cooling, the material was again ground and heated to 1073 K for 45 minutes. The last cycle of hand grinding was done for 30 minutes resulting in a very fine white powder. Pellets of 2-3 mm thickness and approximately 10 mm diameter were

prepared using a die set on a hydraulic pelletizer at a pressure of approximately 70 MPa. The pellets were then batched into three groups. The first group was heated up to 1373 K for 1 hour and allowed to cool slowly. The second batch was heated for 2 hours and the third batch for 3 hours. Details of sample composition are presented in table-1.

All the samples were characterized using X-ray diffraction (XRD), Energy Dispersive Spectroscopy (EDS), density measurements and impedance spectroscopy. Structural characterization of the material was done by X-ray Diffraction (XRD) (Rigaku MiniFlex Cu K α line ($\lambda=1.5405$ Å)). Energy Dispersive Spectroscopy (EDS) using OXFORD EDS analyzer measurements were performed to determine the chemical composition of the compounds. Density was measured using Archimedes principle. Methanol was used as a displacing liquid. The results of EDS are presented in table-2. Impedance measurements were performed in the frequency range of 20 MHz to 1 Hz and temperature range 303 K to 433 K, using the impedance gain/phase analyzer (SOLARTRON 1260). Silver paint was applied on the two surfaces of the pellets to work as electrodes.

RESULTS

The XRD patterns indicate the presence of mixed phases. Apart from the regular LTP phases which have $R\bar{3}c$ rhombohedral structure [1, 2] small amounts of impurity phases like $AlPO_4$ (tridimite), TiO_2 (or TiP_2O_7) rutile phases, YPO_4 and $LiTiPO_5$ are also observed in the XRD patterns. These are indicated by appropriate symbols. Fig. 2(a) and (b) describe the Nyquist (impedance) plots of the two samples at 413 K (140° C) (for two concentrations – 1 wt% and 15wt%) sintered for 1 hour while fig 3 (a) and (b) describe the Nyquist plots of the samples of same concentrations at 413 K but sintered for 3 hours. In the inset of the figures, equivalent circuits used to fit the impedance data from the Equivalent Circuit theory by MacDonald [9, 10] are shown. According to this theory the fitting of the impedance data can be done using a combination of R and C. It is clear that as yttrium concentration and the sintering duration increases, the number of circuit elements used, also increase. This is because as the amount of impurities increase, pure capacitive behavior (C) is replaced by constant phase elements (CPE) [10]. The impedance plots contain two semi circular arcs. At higher frequencies ($> 5 \times 10^4$ Hz) the Li^+ experiences low impedance (and high conductivity) which corresponds to smaller semi circle, which describes the Li^+ conduction in grain region. At lower frequencies, the impedance is higher which indicates the Li^+ motion in grain boundary region. Therefore as the amount of dopant and the sintering duration increases in the samples, the dopants act as impurity phases and block the Li^+ ion transport across the grain and grain boundary regions. The fall of conductivity is also indicated by Arrhenius plots for grain and grain boundary regions (Fig. 4(a) and 4(b) respectively). Highest Li^+ conductivity (5.9×10^{-3} S/cm for grain and 7.2×10^{-4} S/cm at 403 K (130° C) for grain boundary) is obtained for sample S1-H1 (with 1 wt% yttrium and 1 hour sintering duration). It was observed that the grain boundary conductivity (8.4×10^{-5} S/cm at 403 K) improved for S2-H3 sample (with 15 at% yttrium and 3 hours sintering duration) compared to other samples (which is the highest grain boundary conductivity after S1-H1 sample). Thus it can be concluded that there is a marginal improvement in grain boundary conductivity if the sintering duration is enhanced.

DISCUSSION

$Li_{1.3}Al_{0.3-x}Y_xTi_{1.7}(PO_4)_3$ (LATP) has a rhombohedral ($R\bar{3}c$) structure. When trivalent Y^{3+} is doped it tends to replace the trivalent cation Al^{3+} at tetrahedral and octahedral sites within the LATP framework. But Y^{3+} (ionic radii 0.93 Å) is not able to replace Al^{3+} (0.53 Å) due to its massive ionic size. Hence the yttrium oxide present in the grain region tends to settle near the octahedral sites [11]. Due to this, it blocks the pathways for Li^+ migration near the M1 vacancy sites. In octahedral (TiO_6) position it tries to replace Ti^{4+} (0.64 Å) which have a slightly comparable ionic radius. Due to this the Li^+ conductivity is better for sample containing lesser proportion of yttrium. This can be seen from the smaller values of activation energy (table-1). When the samples are sintered at sufficiently high temperatures (1000° C) heavy impurities like YPO_4 tend to segregate at grain boundary [12, 13]. These phases are detected in the XRD patterns as well. They form glassy phases which enhance grain contacts and hence the overall density of the material. This is seen from the increasing values of density (table-1) as a function of sintering duration.

CONCLUSIONS

LATP samples were doped with trivalent cation yttrium for two concentrations (1 at% and 15 at%). These samples were prepared using solid state reaction method. They were sintered for 1, 2 and 3 hours duration at 1373 K to study their microstructure and conductivity. It was concluded that due to dopants, impurity phases are formed which adversely affect the Li^+ conductivity across grain and grain boundary regions. The yttrium phases tend to segregate towards grain boundary as sintering time is increased. Due to this, grain contacts improved. This improved the grain boundary conductivity of sample containing higher proportion of yttrium (and sintered for longer duration of time).

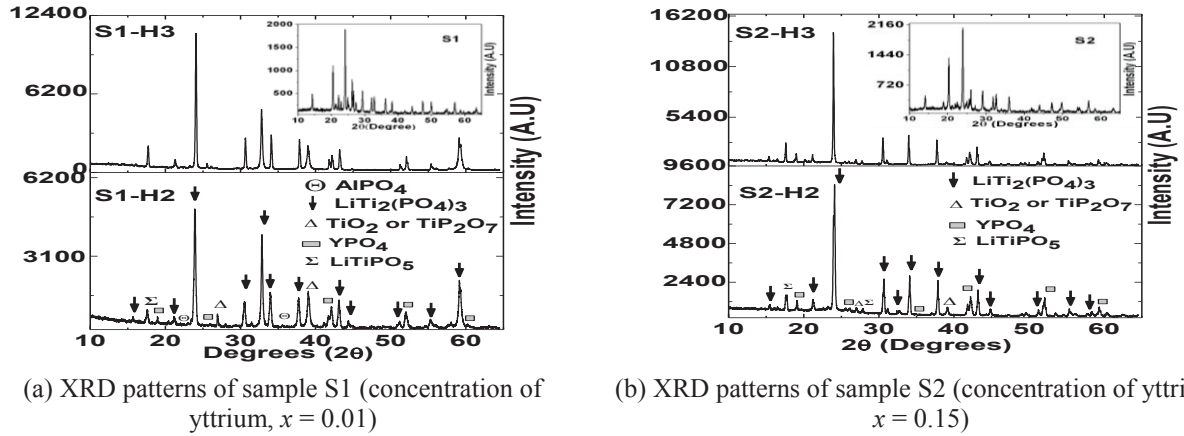


FIGURE 1. XRD patterns of S1 and S2 samples

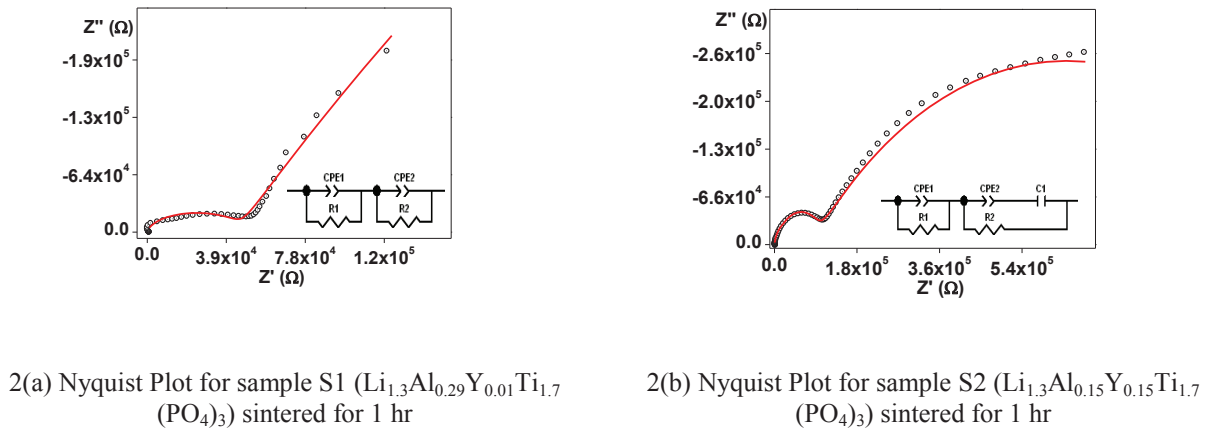
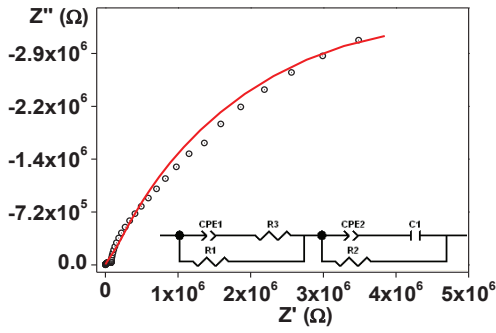
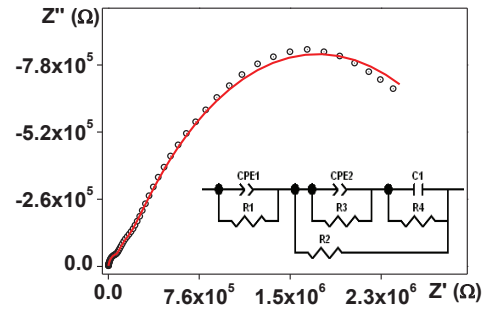


FIGURE 2. Nyquist plots of S1 and S2 samples sintered for 1 hr duration

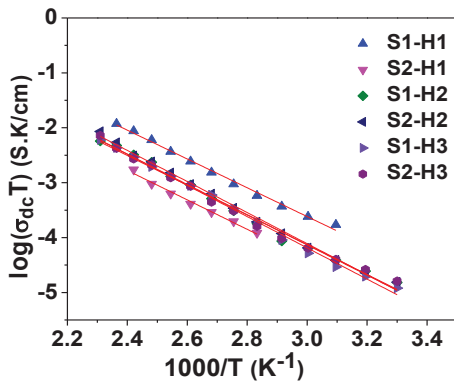


3(a) Nyquist Plot for sample S1 ($\text{Li}_{1.3}\text{Al}_{0.29}\text{Y}_{0.01}\text{Ti}_{1.7}(\text{PO}_4)_3$) sintered for 3 hrs

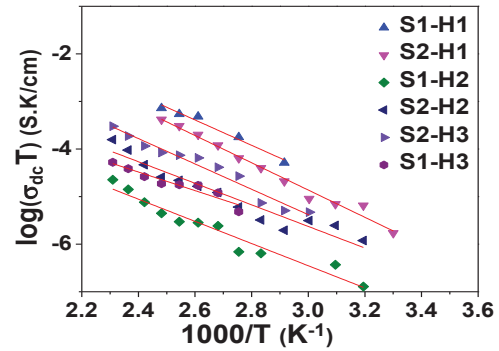


3(b) Nyquist Plot for sample S2 ($\text{Li}_{1.3}\text{Al}_{0.15}\text{Y}_{0.15}\text{Ti}_{1.7}(\text{PO}_4)_3$) sintered for 3 hrs

FIGURE 3. Nyquist plots of S1 and S2 samples sintered for 3 hr duration



4(a) Arrhenius plot for all samples for grain region



4(b) Arrhenius plot for all samples for grain boundary region

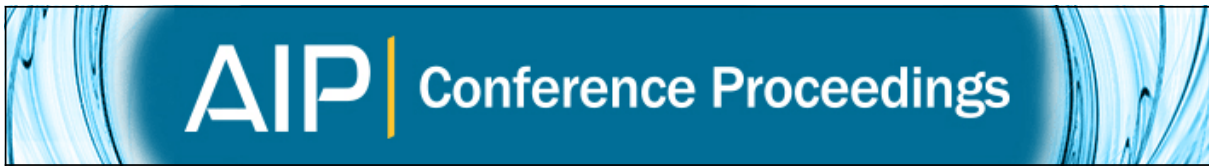
FIGURE 4. Arrhenius Plots of S1 and S2 samples (all concentrations and sintering durations)

TABLE 1. Sample name and compositions, the chemical formula, sintering duration, density, activation energy

Sample Name (x=concentration of Yttrium*)	Chemical Formula	Density (g/cm^3)	Activation Energy (bulk)(eV)
S1-H1 (x= 0.01)	$\text{Li}_{1.3}\text{Al}_{0.29}\text{Y}_{0.01}\text{Ti}_{1.7}(\text{PO}_4)_3$	2.28	0.52
S1-H2 (x= 0.01)	$\text{Li}_{1.3}\text{Al}_{0.29}\text{Y}_{0.01}\text{Ti}_{1.7}(\text{PO}_4)_3$	2.41	0.54
S1-H3 (x= 0.01)	$\text{Li}_{1.3}\text{Al}_{0.29}\text{Y}_{0.01}\text{Ti}_{1.7}(\text{PO}_4)_3$	2.46	0.56
S2-H1 (x= 0.15)	$\text{Li}_{1.3}\text{Al}_{0.15}\text{Y}_{0.15}\text{Ti}_{1.7}(\text{PO}_4)_3$	2.36	0.53
S2-H2 (x= 0.15)	$\text{Li}_{1.3}\text{Al}_{0.15}\text{Y}_{0.15}\text{Ti}_{1.7}(\text{PO}_4)_3$	2.49	0.56
S2-H3 (x= 0.15)	$\text{Li}_{1.3}\text{Al}_{0.15}\text{Y}_{0.15}\text{Ti}_{1.7}(\text{PO}_4)_3$	2.50	0.53

REFERENCES

1. H. Aono, E. Sugimoto, Y. Sadaoka, N. Imanaka, G. Adachi, *Solid State Ionics* **40-41**, 38–42 (1990).
2. G.X. Wang, D.H. Bradhurst, S.X. Dou, H.K. Liu, *J. Power Sources* **124**, 231-236 (2003)
3. H. Aono, E. Sugimoto, Y. Sadaoka, N. Imanaka, G. Adachi, *Chem. Lett.* **10**, 1825–1833 (1990).
4. J. Fu *Solid State Ionics* **96**, 195-201 (1997)
5. D.H. Kothari, D.K. Kanchan, P. Sharma *Ionics* **20(10)**, 1385-1393 (2014)
6. A.F. Orliukas, T. Salkus, A. Kezionis, A. Dindune, Z. Kanepe, J. Ronis, V. Venckute, V. Kazlauskienė, J. Miskinis, A. Lukauskas *Solid State Ionics* **225**, 620-626 (2012)
7. T. Salkus, E. Kazakevicius, A. Kezionis, A. Dindune, Z. Kanepe, J. Ronis, J. Emery, A. Boulant, O. Bohnke, A.F. Orliukas *J. Cond. Matter* **21**, 185502-185508 (2009)
8. T. Salkus, E. Kazakevicius, A. Kezionis, V. Kazlauskienė, J. Miskinis, A. Dindune, Z. Kanepe, J. Ronis, M. Dudek, M. Bucko, J.R. Dugas, W. Bogusz, A.F. Orliukas *Ionics* **16**, 631-640 (2011)
9. J. R. Macdonald, *Fundamentals of Impedance Spectroscopy* (McGraw Hill, New York, 1987) pp. 77–80.
10. J. R. Macdonald *Solid State Ionics* **13**, 147-151 (1984)
11. I. Yu Pinus, A.V. Khoroshilov, K.S. Gavrichev, V.P. Tarasov, A.B. Yaroslavtsev *Solid State Ionics* **212**, 112-117 (2012)
12. M. Shirpour, B. Rahmati, W. Sigle, P.A. Aken, R. Merkle, J. Maier *J. Phys. Chem. C.*, **116**, 2453-2459 (2012)
13. K. Goman, G. Bocharov, M. Schulz, A. Goman, W. Maus-Friedrichs, B. Lesage, O. Kaitasov, S. Hoffman-Eifert, T. Schneller, *Phys. Chem. Chem. Phys.* **7**, 2053-2059 (2005)



Influence of Al₂O₃ nano-filler on dielectric properties and conductivity of two different PVA-PEO blend systems

Prajakta Joge, D. K. Kanchan, and Gargi Dave

Citation: [AIP Conference Proceedings](#) **1665**, 050175 (2015); doi: 10.1063/1.4917816

View online: <http://dx.doi.org/10.1063/1.4917816>

View Table of Contents: <http://scitation.aip.org/content/aip/proceeding/aipcp/1665?ver=pdfcov>

Published by the [AIP Publishing](#)

Articles you may be interested in

[Ion conduction and relaxation in PEO-LiTFSI-Al₂O₃ polymer nanocomposite electrolytes](#)

J. Appl. Phys. **117**, 174103 (2015); 10.1063/1.4919721

[Effect of Al₂O₃ on crystallinity and conductivity of PVA – PEO – EC – LiCF₃SO₃ blend electrolyte system](#)

AIP Conf. Proc. **1591**, 356 (2014); 10.1063/1.4872600

[Effect of EC & LiCF₃SO₃ on conductivity and relaxation in PVA-PEO blends](#)

AIP Conf. Proc. **1512**, 506 (2013); 10.1063/1.4791133

[Role of SnO₂ as a filler in \(PEO\)₅₀AgCF₃SO₃ nanocomposite polymer electrolyte system](#)

AIP Conf. Proc. **1447**, 399 (2012); 10.1063/1.4710048

[Conductivity Studies On PEO: AgCF₃SO₃ Electrolyte System With Nano-porous Fillers](#)

AIP Conf. Proc. **1313**, 177 (2010); 10.1063/1.3530482

Influence of Al₂O₃ Nano-Filler on Dielectric Properties and Conductivity of Two Different PVA-PEO Blend Systems

Prajakta Joge, D. K. Kanchan* and Gargi Dave

Department of Physics, Faculty of Science, The M. S. University of Baroda, Vadodara-390002, India

**E-mail: d_k_kanchan@yahoo.com*

Abstract. System-1: PVA-PEO-PEG-AgNO₃ and System-2: PVA-PEO-EC-LiCF₃SO₃, are two blend systems prepared for different concentrations of Al₂O₃ nano-filler ranging from 2 to 10 wt%. The effect of Al₂O₃ nano filler on the conductivity (σ_{dc}) and dielectric properties such as dielectric constant (ϵ') and dielectric loss (ϵ'') of the systems is thoroughly investigated using impedance spectroscopic analysis technique.

Keywords: Al₂O₃ Nano-Filler, Blend, Impedance spectroscopy, Dielectric, Conductivity.

PACS: 72.80.Tm, 72.80.Le, 73.61.Ph, 77.22.Ch, 77.22.Gm, 77.84.Jd, 77.84.Lf, 81.05.Lg, 81.05.Qk, 82.35.Np, 82.35.Rs, 82.45.Un, 82.45.Gj, 83.80.Ab, 83.80.Tc

INTRODUCTION

Polymer electrolytes are used in various applications such as smart credit cards, cellular phones, fuel cells, batteries, electrochemical devices, laptop, computers, sensors, electrochromic displays, etc. [1]. However, these polymer electrolytes at times depict low values of conductivity which act as a drawback for various applications. Such shortcomings of polymer electrolytes can be minimized upto a certain extent by blending of polymers, plasticization and addition of nano-fillers into electrolytes during their preparation. However, plasticization at times deteriorates the mechanical properties of the polymeric system. Hence, nano-fillers are incorporated into polymer electrolytes which improve mechanical properties as well as conductivity of the system [2, 3] by affecting the free volume of the polymeric matrix, mobility of ions and polymer segments, chain packing, crosslinking density and crystallinity of the matrix, etc. [4]. Additionally, nano-fillers affect the dipole orientation of polymers such as PEO; by their ability to align dipole moments, which enhance the dielectric properties of the polymeric system [5].

Hence, based on the above discussion, two new nano-composite polymer blend systems given as PVA-PEO-PEG-AgNO₃ and System-2: PVA-PEO-EC-LiCF₃SO₃, are prepared and the effect of Al₂O₃ nano-filler on dielectric properties and conductivity of both these systems is investigated in detail. The relationship between conductivity and dielectric properties of both

the systems is explored by comparing the changes occurring in ϵ' and ϵ'' values with the conductivity variation, at different Al₂O₃ concentrations.

EXPERIMENTAL

The two systems given by PVA-PEO-PEG-AgNO₃ (System-1) and PVA-PEO-EC-LiCF₃SO₃ (System-2) are prepared using solution cast technique wherein, the required proportions of PVA, PEO, AgNO₃, LiCF₃SO₃, PEG and EC for the respective systems were added in de-ionized water (solvent) and stirred continuously using magnetic stirrer, for about 24 hours till the solution appeared clear and homogeneous. Later, the thus, obtained solution, was poured in a teflon petridish and kept in a hot air oven for drying at about 45 °C which yielded perfectly dried films in the petridish. The conductivity and dielectric studies of these dried blend films were carried out in the frequency range of 10 Hz to 20 MHz using SOLARTRON 1260 Impedance Gain/Phase Analyzer.

RESULTS AND DISCUSSION

Frequency dependent dielectric measurements provide a better insight regarding the conduction mechanism [3]. Hence, for the present systems, a thorough investigation on dielectric constant (ϵ') and dielectric loss (ϵ'') at various Al₂O₃ concentrations has been done. The Figs. 1 and 2 depict the variation of ϵ' and ϵ'' , respectively, with Al₂O₃ concentration at 333

K for System-1. The variation in ϵ' and ϵ'' , with Al_2O_3 concentration at 333 K for System-2 is shown in Figs. 3 and 4, respectively. Here, the amount of permanent and induced dipole alignment as well as localization of charge carriers (ions) is known by ϵ' whereas, ϵ'' informs about the energy required for the alignment of dipoles as well as for mobility of ions [6, 7]. As observed from Figs. 1-4, for both the systems, the values of ϵ' and ϵ'' are found to be higher at lower frequencies. However, with the increasing frequency, the values of ϵ' and ϵ'' gradually drop and after a certain frequency known as “dispersion frequency”, ϵ' and ϵ'' become almost constant with frequency.

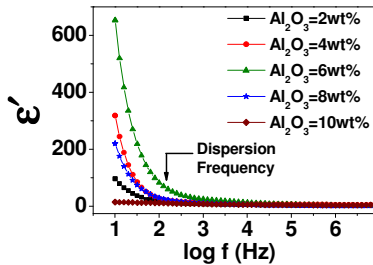


FIGURE 1. ϵ' vs. $\log f$ for various Al_2O_3 concentrations at 333 K for System-1.

At lower frequencies, where frequencies < dispersion frequency, the electric field direction changes slowly owing to which the dipoles of the macromolecules get easily oriented in the direction of electric field. Moreover, the charge carriers also get easily accumulated at the electrode-electrolyte interface and form space charge region, before the direction of electric field changes. This leads to the frequency dependent behavior and higher values of ϵ' and ϵ'' at lower frequencies.

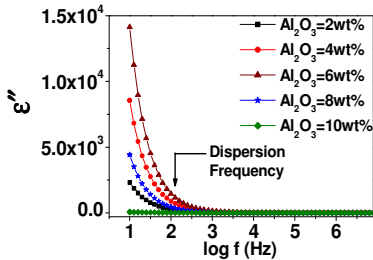


FIGURE 2. ϵ'' vs. $\log f$ for various Al_2O_3 concentrations at 333 K for System-1.

However, as the frequency increases, the electric field direction changes rapidly due to which electric dipoles start lagging behind the electric field. Hence, the orientation of the dipoles with the electric field becomes difficult, leading to a drop in the values of ϵ' and ϵ'' with the increasing frequency. In the high frequency region, where frequencies > dispersion frequency, the periodic reversal of electric field becomes so fast that the dipoles are unable to orient

themselves in the electric field's direction and the charge carriers are incapable to get accumulated at the electrode-electrolyte interface owing to which the ϵ' and ϵ'' values get reduced and become frequency independent.

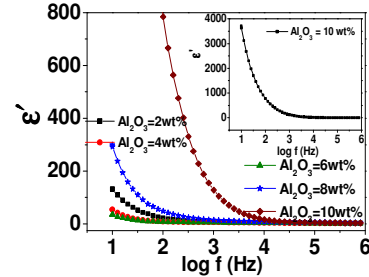


FIGURE 3. ϵ' vs. $\log f$ for various Al_2O_3 amounts (Inset: ϵ' vs. $\log f$ at $\text{Al}_2\text{O}_3=10$ wt%) at 333 K for System-2.

Hence, in order to closely inspect the variation in dielectric properties with Al_2O_3 concentrations in both Systems-1 and 2, the values of ϵ' and ϵ'' corresponding to the lowest frequency i.e. 10 Hz at temperature = 333 K, are selected and shown in Table 1. The variation in ϵ' and ϵ'' values follows the similar trend as depicted by conductivity (σ_{dc}) variation with Al_2O_3 concentrations in Fig. 5. ϵ' and ϵ'' values as well as conductivity for System-1 increase systematically with Al_2O_3 content upto 6 wt%, but reduce gradually with Al_2O_3 amount above 6 wt% whereas; in System-2, ϵ' and ϵ'' values and conductivity drop initially with increasing Al_2O_3 amount upto 6 wt% but enhance beyond 6 wt% of Al_2O_3 . Additionally, as seen from Figs. 1-4, dispersion frequency also shifts with the filler concentration. In case of System-1, the dispersion frequency gradually shifts towards higher frequency side with increasing Al_2O_3 concentration upto 6 wt%, but at Al_2O_3 beyond 6 wt%, the shift is towards the lower frequency side. The reverse is observed for System-2 wherein, dispersion frequency moves towards lower frequency region upto 6 wt% of Al_2O_3 but with further increment of filler amount, the shift is towards the opposite side. The increment in Al_2O_3 upto 6 wt% in System-1 gradually increases the free volume and flexibility of the matrix by making the system amorphous. This promotes the mobility of Ag^+ and NO_3^- ions and polymer segments through the matrix. This discussion is clearly understood by the increment in the values of ϵ' , ϵ'' and σ_{dc} as well as by the shift in the dispersion frequency towards higher frequency side with Al_2O_3 content upto 6 wt%. However, beyond 6 wt% of Al_2O_3 the values of ϵ' , ϵ'' and σ_{dc} drop and the dispersion frequency shifts towards lower frequency side. This may be due to the formation of filler aggregates which in turn block conducting pathways and reduce the free volume of blend matrix by making system crystalline,

TABLE 1. Variation in ϵ' and ϵ'' with Al_2O_3 concentrations in System-1 and System-2 at frequency = 10 Hz and temperature = 333 K.

Al_2O_3 (wt%)	ϵ' for System-1	ϵ' for System-2	ϵ'' for System-1	ϵ'' for System-2
2	96.47	133.16	2309.11	634.86
4	318.78	54.73	8558.63	385.37
6	651.88	35.32	14136.97	234.46
8	219.55	299.31	4424.87	1466.16
10	15.29	3714.58	72.53	4498.14

owing to which the motion of Ag^+ and NO_3^- ions and polymer segments through the matrix reduces. Additionally, the variation of ϵ' and ϵ'' values with Al_2O_3 content in System-1 also suggests that the alignment of dipoles, localization of Ag^+ and NO_3^- ions as well as the energy required for alignment of dipoles and mobility of ions also gradually increase with the Al_2O_3 amount upto 6 wt%, but reduce beyond 6 wt% of Al_2O_3 . On the contrary, the reverse may have occurred in System-2 wherein the dispersion frequency shifts towards lower frequency side and ϵ' , ϵ'' and σ_{dc} values reduce with increasing Al_2O_3 amount upto 6 wt%. In this case, initially, with increasing filler concentration, the aggregation of the filler particles may have taken place which gradually increased the crystallinity of the blend matrix, blocked the conducting pathways and thus, obstructed the mobility of Li^+ and CF_3SO_3^- ions. Also, the dipole alignment, charge carrier localization as well as the energy required in the dipole alignment and ion mobility reduces with filler content upto 6 wt%. Hence, ϵ' , ϵ'' and σ_{dc} values drop and the dispersion frequency shift towards lower frequency side with increasing Al_2O_3 content upto 6 wt%. However, at $\text{Al}_2\text{O}_3 > 6$ wt% the ϵ' , ϵ'' and σ_{dc} values enhance and the dispersion frequency shifts towards higher frequency side. This may be due to the initiation of the process of free volume formation owing to the increasing amorphicity of the matrix beyond 6 wt% of Al_2O_3 , which in turn makes the system flexible. This increases the mobility of Li^+ and CF_3SO_3^- ions and polymer segments through the matrix, dipole alignment, charge carrier localization as well as energy required in the dipole alignment and ion mobility. Hence, ϵ' , ϵ'' and σ_{dc} values enhance and dispersion frequency shifts towards higher frequency side at $\text{Al}_2\text{O}_3 > 6$ wt%.

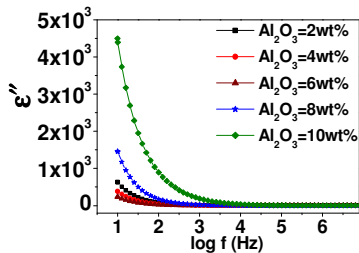


FIGURE 4. ϵ'' vs. $\log f$ for various Al_2O_3 concentrations at 333 K for System-2.

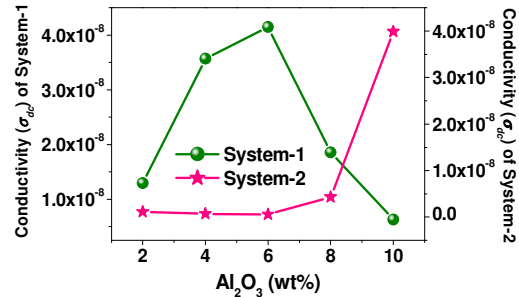


FIGURE 5. Conductivity (σ_{dc}) vs. Al_2O_3 concentrations at 323 K for System-1 and System-2.

CONCLUSION

Likewise the conductivity variation, the dielectric properties of PVA-PEO-PEG- AgNO_3 system enhance gradually upto 6 wt% of Al_2O_3 but worsen at $\text{Al}_2\text{O}_3 > 6$ wt% whereas; in PVA-PEO-EC- LiCF_3SO_3 system the conductivity and dielectric properties which deteriorate systematically with Al_2O_3 content upto 6 wt%, improve significantly at $\text{Al}_2\text{O}_3 > 6$ wt%. Hence, the specimens with 6 wt% of Al_2O_3 of PVA-PEO-PEG- AgNO_3 system and with 10 wt% of Al_2O_3 of PVA-PEO-EC- LiCF_3SO_3 system show the best conductivity as well as dielectric properties.

REFERENCES

1. P. Joge, D. K. Kanchan, P. Sharma, M. Jayswal and D.K. Avasthi, *Radiation Physics and Chemistry* **100**, 74–79 (2014).
2. P. Sharma, D. K. Kanchan, N. Gondaliya, M. Jayswal and P. Joge, *Indian Journal of Pure and Applied Physics* **51**, 346-349 (2013).
3. D. K. Ray, A. K. Himanshu and T. P. Sinha, *Indian Journal of Pure and Applied Physics* **45**, 692-699 (2007).
4. G. Choudalakis and A.D. Gotsis, *Current Opinion in Colloid & Interface Science* **17**, 132-140 (2012).
5. N. Gondaliya, D. K. Kanchan, P. Sharma and P. Joge, *Journal of Applied Polymer Science* **125**, 1513–1520 (2012).
6. I. B. Amor, H. Rekik, H. Kaddami, M. Raihane, M. Arous and A. Kallel, *Journal of Electrostatics* **67**, 717-722 (2009).
7. K. Mohamed, T. G. Gerasimov, F. Moussy and J. P. Harmon *Polymer* **46**, 3847-3855 (2005).